

Original Paper

Geochemical Characteristics of Oil from Oligocene Lower Ganchaigou Formation Oil Sand in Northern Qaidam Basin, China

Ye Liang,^{1,2} Xuanlong Shan ,^{1,7} Yousif M. Makeen,¹ Wan Hasiah Abdullah,² Guoli Hao,¹ Lihua Tong,^{3,4} Mutari Lawal,^{2,5} Rongsheng Zhao,¹ and Habeeb A. Ayinla⁶

Received 19 November 2018; accepted 6 February 2019
Published online: 15 February 2019

Oil from the Oligocene oil sands of the Lower Ganchaigou Formation in the Northern Qaidam Basin and the related asphaltenes was analyzed using bulk and organic geochemical methods to assess the organic matter source input, thermal maturity, paleo-environmental conditions, kerogen type, hydrocarbon quality, and the correlation between this oil and its potential source rock in the basin. The extracted oil samples are characterized by very high contents of saturated hydrocarbons (average 62.76%), low contents of aromatic hydrocarbons (average 16.11%), and moderate amounts of nitrogen–sulfur–oxygen or resin compounds (average 21.57%), suggesting that the fluid petroleum extracted from the Oligocene oil sands is of high quality. However, a variety of biomarker parameters obtained from the hydrocarbon fractions (saturated and aromatic) indicate that the extracted oil was generated from source rocks with a wide range of thermal maturity conditions, ranging from the early to peak oil window stages, which are generally consistent with the biomarker maturity parameters, vitrinite reflectance (approximately 0.6%), and T_{max} values of the Middle Jurassic carbonaceous mudstones and organic-rich mudstone source rocks of the Dameigou Formation, as reported in the literature. These findings suggest that the studied oil is derived from Dameigou Formation source rocks. Furthermore, the source- and environment-related biomarker parameters of the studied oil are characterized by relatively high pristane/phytane ratios, the presence of tricyclic terpanes, low abundances of C_{27} regular steranes, low C_{27}/C_{29} regular sterane ratios, and very low sterane/hopane ratios. These data suggest that the oil was generated from source rocks containing plankton/land plant matter that was mainly deposited in a lacustrine environment and preserved under sub-oxic to oxic conditions, and the data also indicate a potential relationship between the studied oil and the associated potential source rocks. The distribution of pristane, phytane, tricyclic terpanes, regular steranes and hopane shows an affinity with the studied Oligocene Lower Ganchaigou Formation oil to previously published Dameigou Formation source rocks. In support of this finding, the pyrolysis–gas chromatography results of the analyzed oil asphaltene indicate that the oil was primarily derived from type II organic matter, which is also consistent with the organic matter of the Middle Jurassic source rocks. Thus, the Middle Jurassic carbonaceous

¹College of Earth Sciences, Jilin University, No. 2199, Jianshe Street, Changchun 130061, China.

²Department of Geology, University of Malaya, 50603 Kuala Lumpur, Malaysia.

³Oil and Gas Survey, China Geological Survey, Beijing 10083, China.

⁴The Key Laboratory of Unconventional Petroleum Geology, CGS, Beijing 100083, China.

⁵Department of Geology, Usmanu Danfodiyo University Sokoto, P.M.B. 2346 Sokoto, Nigeria.

⁶Department of Geology, Federal University, P.M.B. 1154 Lokoja, Nigeria.

⁷To whom correspondence should be addressed; e-mail: shanxl@jlu.edu.cn

mudstones and organic rock mudstones of the Dameigou Formation could be significantly contributing source rocks to the Oligocene Lower Ganchaigou Formation oil sand and other oil reservoirs in the Northern Qaidam Basin.

KEY WORDS: Origin and type of organic matter, Paleo-environmental conditions, Oil–source rock correlation.

INTRODUCTION

As global energy demands continue to increase, hydrocarbon exploration and development will be driven from crude oil toward unconventional forms of energy. Oil sands, as an unconventional energy source, are considered enormous energy resources in the global inventory of petroleum reserves despite their controversial and undesirable features, such as their increased oil viscosity, acidity, and sulfur content (Larter and Douglas 1980; Tenenbaum 2009). Oil sands (also known as asphaltic sands or tar sands) are sedimentary rocks (mostly sandstone or carbonate) that contain heavier oil or bitumen. Oil sands form due to the low-temperature alteration of crude oil, biodegradation, light-hydrocarbon volatilization, or water washing as a result of the concentration of high molecular weight hydrocarbon, resins, and asphaltenes (Gao et al. 2005). Oil sand layers often exist at shallow depths in a basin or are exposed at the Earth's surface by tectonic uplift and weathering (Niu and Hu 1999; Gao et al. 2005; CAPP (Canadian Association of Petroleum Producers) 2017).

With the development of horizontal drilling and steam-assisted gravity drainage (SAGD) techniques for the enhanced oil recovery of heavy crude oil and bitumen, oil sand has become an important contributor to the global energy supply (Sudiptya and Berna 2018). Globally, Canada, the USA, and Venezuela (the richest oil sand countries) have used different exploitation methods of oil sands since the twentieth century (CAPP 2017). For example, in Canada, asphalt and oil extracted from oil sands now represent approximately half of the total liquid petroleum composition (EIA 2012). Thus, more investigation and exploration of oil sands as an unconventional energy resource are required.

In China, oil sand reservoirs are charged predominantly from lacustrine source rocks. Several basins in China have been reported to have large-

scale occurrences of oil sands, including the Qaidam, Ordos, Bohai Bay, and Sichuan basins (Fig. 1) (Wang et al. 2015). China's first tight oil discovery, the Xin'anbian Oilfield in the Ordos Basin, is credited with over 1 billion tons of 3P reserves (proved reserves, probable reserves, and possible reserves) and an annual production of up to 101 million tons (Wang et al. 2015).

The study area (i.e., the Northern Qaidam Basin), which contains 4.94×10^8 t of oil sand resources and 2.94×10^8 t of recoverable resources, is the fourth-largest oil sand-bearing basin in China (Niu and Hu 1999). Research on the conventional oil system of the Qaidam Basin has been well documented, and a number of studies have focused on its reservoir (Feng et al. 2013; Li et al. 2015), source rocks (Qin et al. 2018), geochemistry (Huang et al. 1994; Duan et al. 2006), and petroleum accumulation (Guo et al. 2018). However, little attention has been paid to the geochemical characteristics of oil sands in conjunction with their potential source rocks in the Qaidam Basin except for the physical and chemical characteristics of the oil sands reported by Gao et al. (2005). These authors characterized oil sands based on their viscosity, density, and sedimentary environment. This lack of research has restricted the exploration and development of oil sands in the Qaidam Basin.

Additionally, studies of the oil sand geochemistry in the Northern Qaidam Basin, which can largely reduce the risk of petroleum exploration, such as oil–source rock correlations based on biomarker analysis (Makeen et al. 2015c; Manzano et al. 2016), assessments of depositional environment conditions using biomarker and element analyses (Marek et al. 2013; Makeen et al. 2015d; Huang et al. 2016), and determinations of the stage of biodegradation (Zhou et al. 2008; Makeen et al. 2015c; Park et al. 2018), are lacking.

The objectives of this study are to assess the origin and type of organic matter, thermal maturity, and depositional environment of source rock using

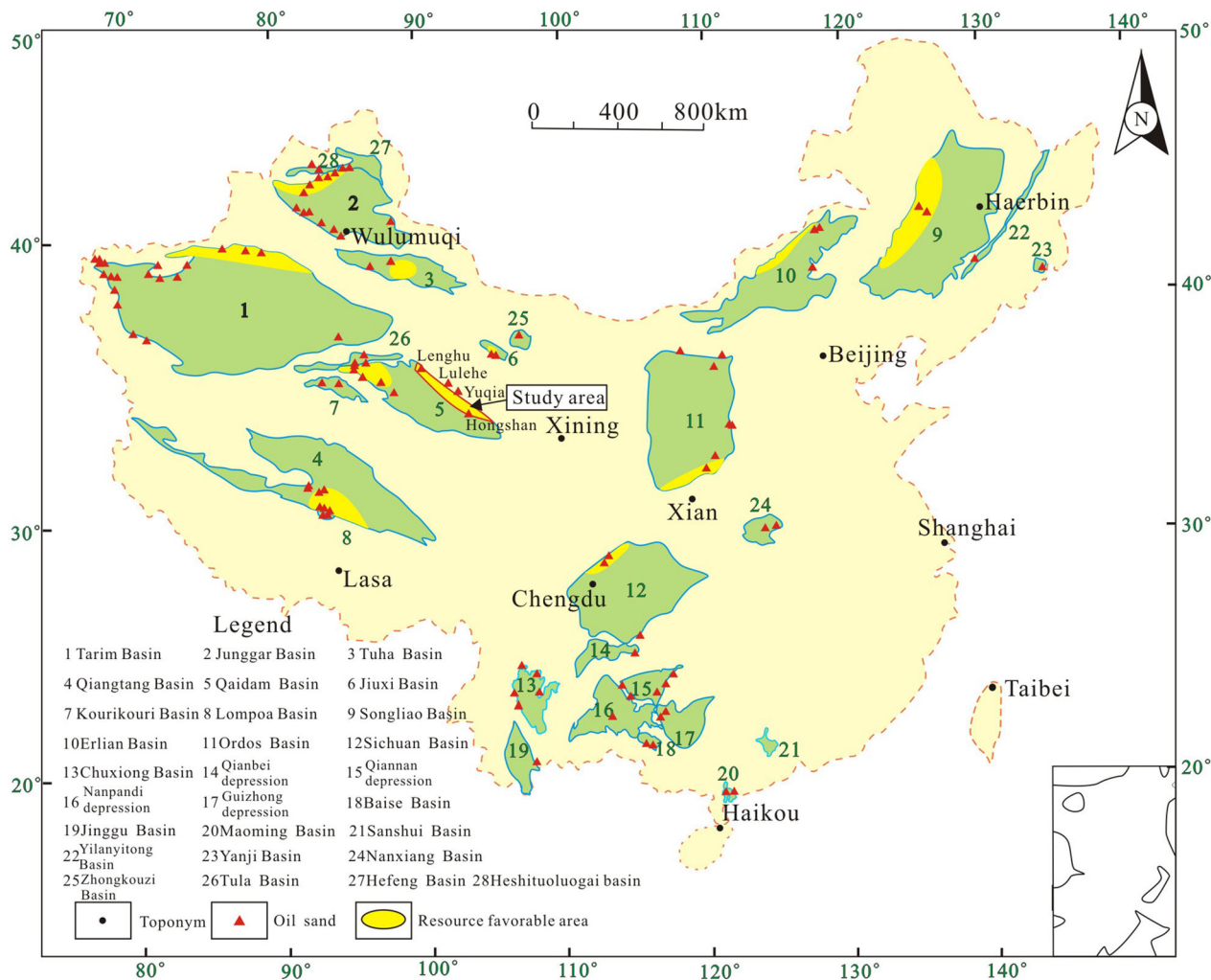


Figure 1. Geological map showing the location of the study area and the distribution of oil sand-bearing basins in China (modified after the Oil and Gas Resources Survey Center of the China Geological Survey 2009).

liquid column chromatography and gas chromatography–mass spectrometry (GC–MS), gas chromatography double mass spectrometry (GC–MS/MS), inductively coupled plasma mass spectrometry (ICP–MS), and pyrolysis–gas chromatography (Py–GC). Oil–source rock correlations were also determined to establish the genetic relationship between the studied oil and its related potential source rocks. The outcome of this study will enhance the understanding of the oil–source correlation and increase the hydrocarbon exploration activity related to oil sand in China, including the Northern Qaidam Basin (Fig. 1).

GEOLOGICAL SETTING

The Qaidam Basin is the largest intermountain basin in the northern Tibetan Plateau and has a maximum area of approximately 120,000 km² (Métivier et al. 1998; Lu et al. 2018). It is bounded by three major mountain ranges: the Qilian Mountains to the northeast, the Altun Mountains to the northwest, and the Kunlun Mountains to the south (Fig. 2a). The study area of this project is located in the northern part of the Qaidam Basin (Fig. 2b).

Tectonically, the Qaidam Basin is divided into four structural units based on differences in topog-

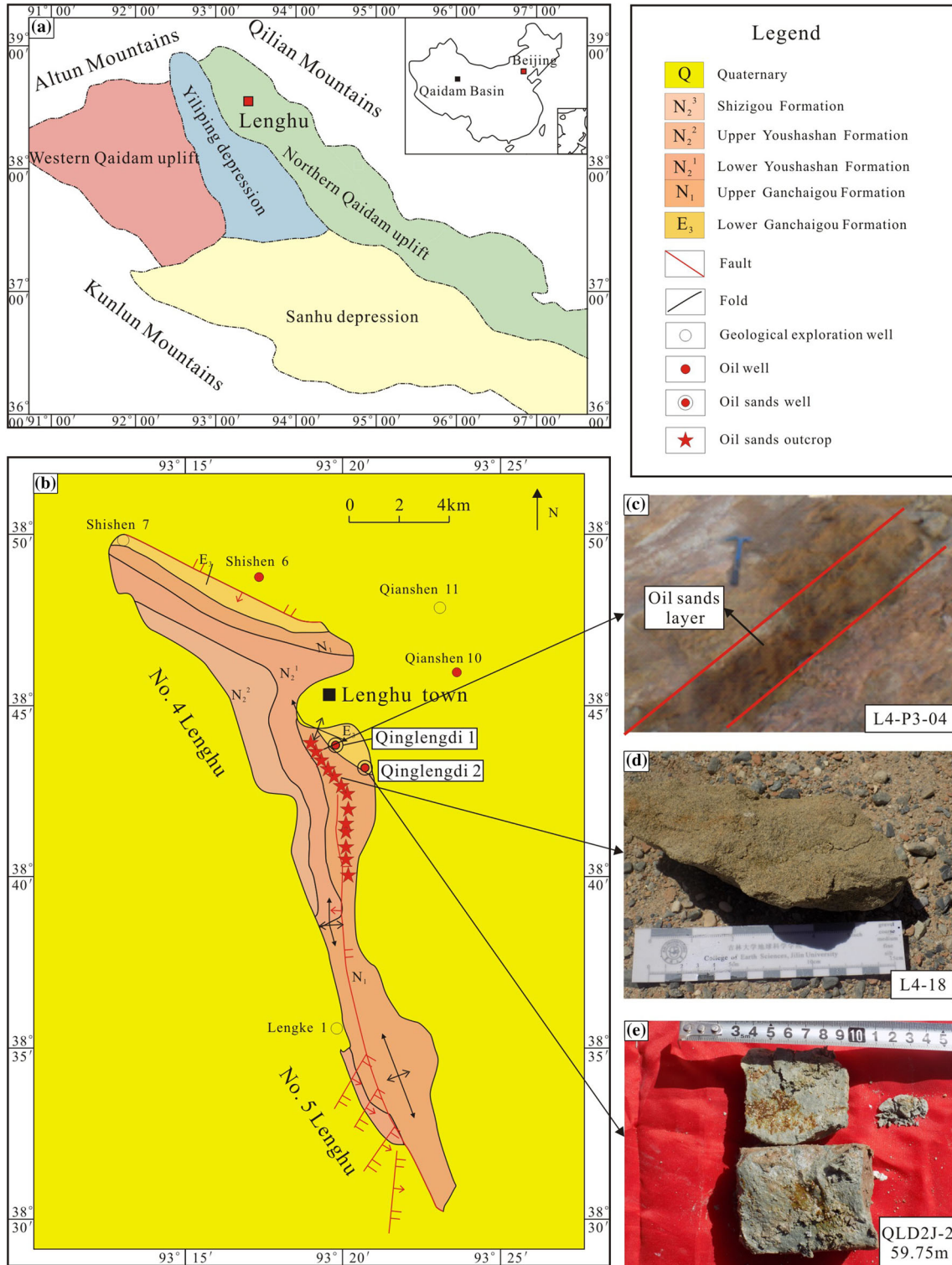


Figure 2. Basic geological information about the oil sands in the Lower Ganchaigou Formation in the Northern Qaidam Basin. (a) Location map of the Qaidam Basin showing the study area; (b) geological map of the Northern Qaidam Basin (study area) showing structure, strata, and oil sand outcrop and drilling locations; (c) example of an oil sand layer in the study area; (d) oil sand sample obtained from outcrop; and (e) oil sand sample obtained from drilling.

raphy, namely the Sanhu depression, the northern Qaidam uplift, the Yiliping depression, and the western Qaidam uplift (Mao et al. 2016; Bao et al. 2017). The study area is located in the northern Qaidam uplift (Fig. 2a). The basin has experienced three stages of sedimentary evolution, namely the Late Triassic–Late Cretaceous breakage period, the Paleogene–Early Neogene depression period, and the Late Neogene–Early Pleistocene return period (Zhou et al. 2006; Yin et al. 2008; Du et al. 2018).

The Cenozoic strata exposed in the Northern Qaidam Basin are divided into seven formations (Fms), which include (from bottom to top) the Lulehe Fm, the lower and upper Ganchaigou Fms, the lower and upper Youshashan Fms, the Shiziou Fm, and the Qiqequan Fm (Fig. 3; Lu and Xiong 2009; Wang et al. 2012). Earlier studies provided detailed analyses of their invertebrate ostracods, fossil mammals, lithostratigraphic correlations, and magnetostratigraphy (Meng et al. 2001; Mischke et al. 2010; Ji et al. 2017).

The Lower Ganchaigou Fm is the main reservoir in the Qaidam Basin, and it is composed of fine and dark lithologies, including a set of gray and dark gray mudstone, calcareous mudstone, gypsum-bearing mudstone, argillaceous siltstone, carbonate, and gypsum–salt rock (Yi et al. 2017). Based on the characteristics of its lithological assemblage, it can be divided into two sections: the lower part, which is mainly red coarse clastic rock deposits with brown-red sandy conglomerate and mudstone lithologies indicative of an alluvial fan depositional environment that experienced drought, and the upper part, which consists of gray mudstone, marl, and fine sandstone with carbonate interlayers indicative of stable lacustrine depositional conditions. The thickness of this formation is in the range of approximately 182–2000 m (Li et al. 2017). The grain size fines upward as the environment shows a transition from fan-delta to delta-lacustrine conditions. The oil sands in the study area are mainly gray medium- to pebble-grained sandstone from the upper part of the Lower Ganchaigou Fm, with the occurrence of oil trapped in pore spaces (Fig. 2c, d, and e).

Previous studies suggested that the main source rocks in the Qaidam Basin are from the Lower and Middle Jurassic sequences (Qin et al. 2018). The Lower Jurassic source rock lithology is divided into coal and carbonaceous mudstones, whereas the Middle Jurassic source sequences mainly contain carbonaceous mudstone and dark mudstone, with thin sandstone and coal layers. The quality of the

Middle Jurassic source rock is better than that of the Lower Jurassic source rock (Shu et al. 2017).

The Middle Jurassic Dameigou Fm in the Northern Qaidam Basin has long been the subject of numerous studies due to its important hydrocarbon source potential (e.g., Qin et al. 2018). The Dameigou Fm has been divided into seven sedimentary facies members (Feng et al. 2013). The first, second, and third members were formed during the Lower Jurassic. The first member mainly consists of carbonaceous mudstone and oil shale facies, while the second and third members consist of lean organic-rich mudstone and sandstone facies. The other four members were deposited during the Middle Jurassic, including thick sandstone deposits from members four to six and relatively thick lacustrine sediments with thin layers of carbonaceous mudstone and organic-rich mudstone in the seventh member (Qin et al. 2018) (Fig. 3).

DATASET AND METHODS

The sample set in the present study includes 13 outcrop samples and 13 core samples collected from the No. 4 Lenghu area in the Northern Qaidam Basin (Fig. 2b). The locations of the samples are shown in Figure 2b. The core samples are taken from two newly drilled wells (Qinglengdi 1 and Qinglengdi 2) (Figs. 2b and 4) with subsurface depths ranging from 0 to 300 m (Fig. 4). All of these samples were subjected to conventional column chromatography to separate their hydrocarbon (saturated and aromatic), NSO, and asphaltene compounds (Table 1).

Approximately 20 g of each powdered oil sand sample was placed into a thimble, covered with cotton, and then placed in a Soxhlet apparatus. Two hundred milliliters of an azeotropic mixture of 87% chloroform and 13% methanol was placed in a 250-ml flat-bottom flask connected to the Soxhlet apparatus that was attached to a condensing chamber. Anti-bumping granules and copper sheets were added to the solvent in the flask, while the condensing chamber was connected to the water inlet and outlet to cool the system. This reflux procedure lasted for 72 h to ensure exhaustive extraction. The liquid achieved was concentrated by evaporation until it reached a constant weight using a rotary evaporator.

Liquid column chromatography on silica gel (60–210 mesh) topped with alumina oxide was used to divide the extracted oil from oil sands by frac-

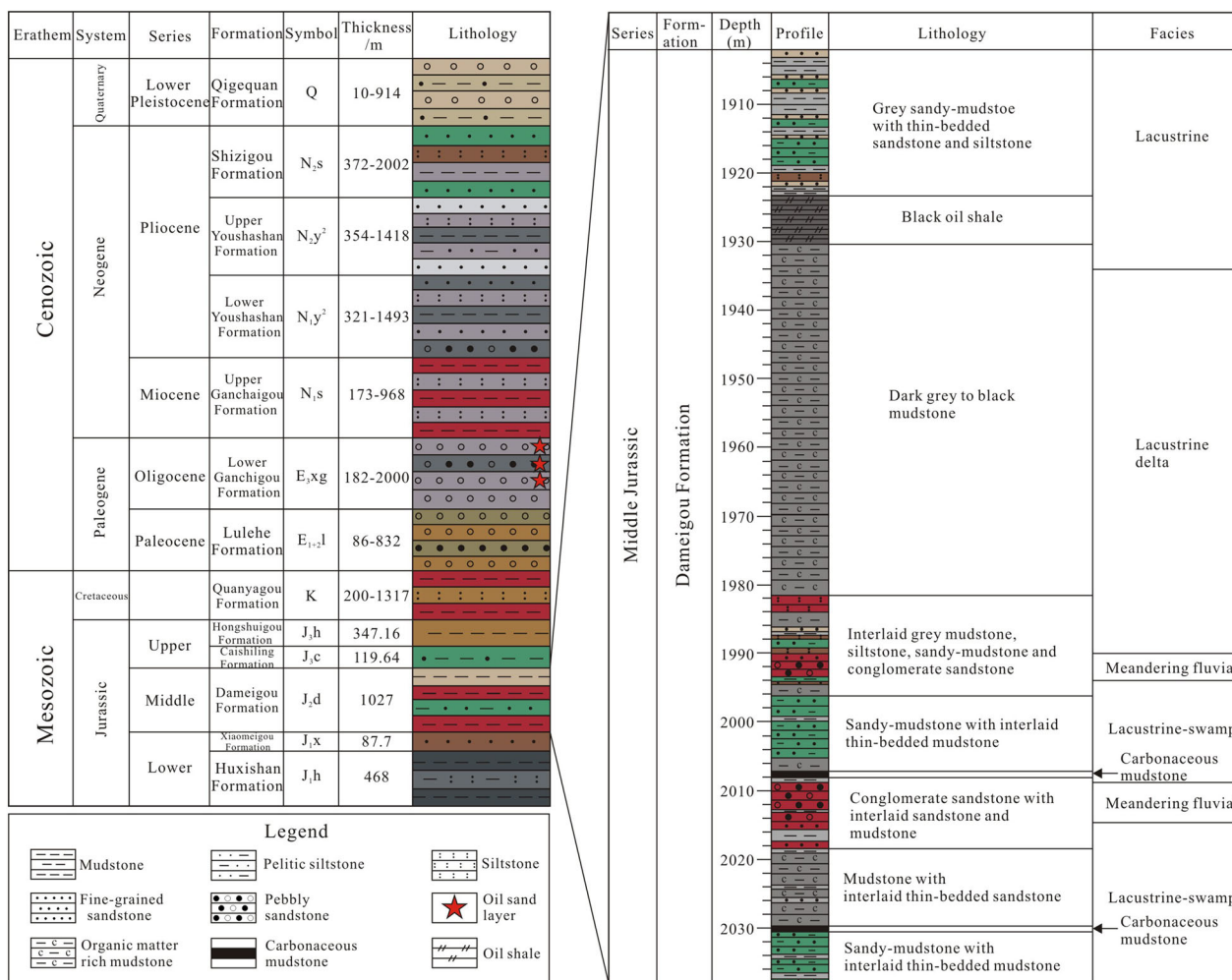


Figure 3. Stratigraphic column of the Northern Qaidam Basin strata showing oil sands of the Oligocene Lower Ganchaigou Formation and the Middle Jurassic Dameigou Formation source rocks (modified after Qin et al. 2018).

tionation (saturated, aromatic, and NSO compounds). Prior to the commencement of this analysis, alumina and silica, which form the stationary phase during this separation, were activated by keeping them in the oven at 110 °C. Three different solvents of increasing polarity in the sequential order of petroleum ether (100 ml), dichloromethane (100 ml), and methanol (50 ml) were used to extract saturated hydrocarbons, aromatic hydrocarbons, and NSO compounds, respectively. After concentrating the eluents in a Buchi rotary evaporator and drying them, the weights of the different fractions were determined and recorded.

The eluate hydrocarbon (saturated and aromatic) fractions were analyzed using an Agilent

5975B inert MSD mass spectrometer with a gas chromatograph (GC) attached to the ion source (with an ionization voltage of 70 eV, filament emission current of 100 mA, and interface temperature of 230 °C). The analysis was performed using a 30-m-long, 0.32-mm-internal-diameter HP-5MS column. Approximately 1 µl of each hydrocarbon fraction (mixed with *n*-hexane) was injected with the aid of a standard golden syringe into the gas fragmentogram inlet. Fused silica and helium were the stationary and mobile phases, respectively, during the separation. Some of the selected peaks, such as those of *n*-alkanes, tricyclic terpanes, hopanes, and steranes, were identified based on their retention time and comparison with identifications by previous

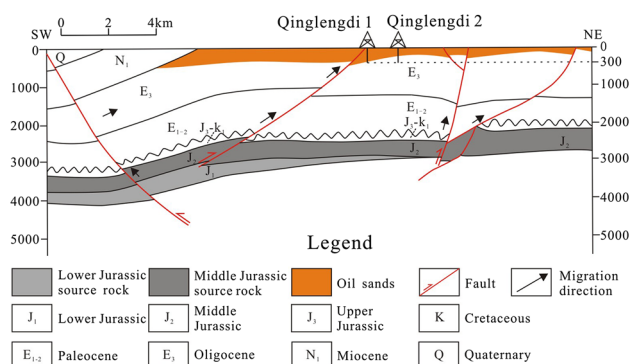


Figure 4. Geological cross section of the Lenghu area in the Northern Qaidam Basin showing the depth of the drilled wells in the Lenghu area (modified from Tian et al. 2018).

researchers (e.g., Peters and Moldowan 1993; Peters et al. 2004; Hakimi et al. 2011; Makeen et al. 2015a, b). A GC–MS/MS analysis was performed on selected oil samples to assess specific biomarkers using an Agilent 7890B GC equipped with a tandem 7000B triple quadrupole MS/MS system; in this, the MS column consists of two scanning mass analyzers separated by a collision cell. Fragments selected in the first analyzer are reacted with an inert gas in the collision cell, resulting in further fragmentation. The heating process involved heating at 70 °C for 3 min, then increasing by 5 °C/min to 200 °C, then increasing by 4 °C/min to 320 °C, which was held there for 20 min (with a total run time of 79 min) (Etxebarria et al. 2009; Mei et al. 2018). The electron impact (EI) ion source for the triple quadrupole mass spectrometer was operated in multiple reaction monitoring (MRM) mode under the conditions of 70 eV and 230 °C, and the quadrupoles were operated at 150 °C.

Following the GC–MS and GC–MS/MS analyses, a pyrolysis GC analysis was performed on approximately 2 mg of selected precipitated asphaltene from each oil sample using a Frontier Lab Pyrolyser System, which was attached to an inert column (quartz and Ultra ALLOY-5) (length of 30 m, internal diameter of 0.25 mm, and film thickness of 0.52 μm) fitted to an Agilent GC chromatograph equipped with a flame ionization detector. During this process, the pyrolysate was monitored between 300 and 600 °C (25 °C/min). The generated chromatogram peaks of interest were identified based on their retention time and comparison to published works (e.g., Makeen et al. 2015c).

An ICP–MS analysis was carried out on approximately 0.5 g of each oil sample to determine

the concentrations of major and trace elements in the Northern Qaidam Basin. Representative samples were passed through a digestion process to dissolve their constituent elements in a liquid medium in readiness for ICP–MS analysis. To achieve total digestion, the samples were heated in a mixture of HNO₃, HClO₄, and HF to fuming and taken to dryness. The residue of each sample was dissolved in HCl. The minimum and maximum detection limits of the equipment are 0.5 ppb and 100%, respectively. The method used was previously described by Pi et al. (2013) and Adegoke et al. (2014).

RESULTS

Column Chromatographic Extraction

The ratio of hydrocarbon to non-hydrocarbon components separated by column chromatography can be used to provide a better interpretation of oil/source rock quality (Peters and Moldowan 1993). In this study, the saturated and aromatic components represent the major fractions of the analyzed oil samples (Table 1). The relative proportions of the saturated and aromatic fractions ranged from 32.60 to 89.00% and 3.27 to 27.64%, respectively, while those of the NSO fractions ranged from 4.42 to 55.32% (Table 1 and Fig. 5).

n-Alkanes and Isoprenoids

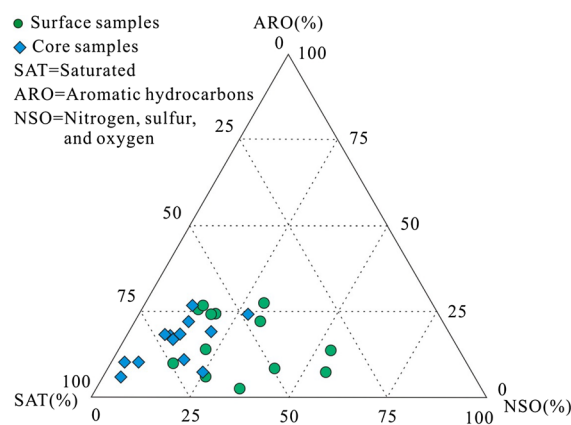
Detailed biomarker studies were conducted based on the normal alkane and isoprenoid distributions determined using GC–MS based on moni-

Table 1. Bulk geochemical results of liquid column chromatography, relative proportions of hydrocarbons (saturated and aromatic), and NSO compounds (in wt.%) of the analyzed oil samples

No.	Sample ID	Lithology	Depth/m	Bitumen yield and chromatographic fractions (g of whole samples)					Chromatographic fractions of bitumen extraction (oil wt.%)				
				Oil	Sat.	Aro.	NSO	HCs	Sat.	Aro.	NSO	HCs	Sat/Aro%
1	L4-02	Sandstone	0	0.070	0.021	0.009	0.035	0.030	32.60	13.40	54.00	46.00	2.4
2	L4-05	Sandstone	0	0.032	0.015	0.002	0.004	0.017	50.50	7.31	42.19	57.81	6.9
3	L4-07	Sandstone	0	0.036	0.020	0.009	0.006	0.029	57.20	24.50	18.30	81.70	2.3
4	L4-10	Sandstone	0	0.035	0.011	0.002	0.006	0.013	37.23	7.45	55.32	44.68	5.0
5	L4-18	Sandstone	0	0.072	0.019	0.009	0.013	0.028	46.30	22.30	31.40	68.60	2.1
6	L4-21	Sandstone	0	0.101	0.063	0.003	0.025	0.066	62.00	3.27	34.72	65.28	18.9
7	L4P2-01	Sandstone	0	0.066	0.037	0.015	0.012	0.052	58.04	23.58	18.38	81.60	2.5
8	L4P2-02	Sandstone	0	0.034	0.019	0.008	0.004	0.027	61.26	25.63	13.11	86.90	2.4
9	L4-P3-02	Sandstone	0	0.056	0.029	0.009	0.009	0.038	61.00	19.20	19.80	80.20	3.2
10	L4-P3-04	Sandstone	0	0.038	0.005	0.010	0.007	0.016	43.30	26.20	30.50	69.50	1.7
11	LH4H-01	Sandstone	0	0.227	0.142	0.012	0.018	0.155	68.59	5.97	25.43	74.57	11.5
12	LH4H-02	Sandstone	0	0.030	0.016	0.003	0.005	0.020	65.03	14.09	20.88	79.10	4.6
13	LH4H-04	Sandstone	0	0.116	0.082	0.011	0.011	0.093	74.14	9.80	16.06	83.94	7.6
14	QLD1J-11	Sandstone	159.55	0.059	0.042	0.010	0.004	0.051	71.80	16.96	11.25	88.75	4.2
15	QLD1J-12	Sandstone	174.2	0.042	0.029	0.007	0.003	0.036	71.64	17.41	10.95	89.05	4.1
16	QLD1J-13	Sandstone	174.15	0.038	0.024	0.006	0.002	0.030	71.99	18.37	9.64	90.36	3.9
17	QLD1J-14	Sandstone	207.3	0.035	0.023	0.006	0.003	0.029	69.49	18.13	12.39	87.61	3.8
18	QLD2J-1	Sandstone	5.54	0.038	0.027	0.004	0.002	0.031	72.40	11.75	15.85	84.15	6.2
19	QLD2J-2	Sandstone	31.97	0.039	0.022	0.010	0.004	0.032	59.35	27.64	13.01	86.99	2.1
20	QLD2J-4	Sandstone	59.75	0.033	0.015	0.008	0.005	0.022	48.38	24.35	27.27	72.73	2.0
21	QLD2J-11	Sandstone	78.35	0.085	0.044	0.003	0.002	0.047	89.00	6.52	4.48	95.52	13.7
22	QLD2J-16	Sandstone	125.65	0.075	0.043	0.019	0.007	0.062	62.09	26.61	11.30	88.70	2.3
23	QLD2J-18	Sandstone	147.15	0.053	0.033	0.011	0.006	0.044	65.09	22.29	12.62	87.38	2.9
24	QLD2J-29	Sandstone	186.9	0.185	0.153	0.018	0.005	0.171	85.46	10.12	4.42	95.58	8.4
25	QLD2J-35	Sandstone	235.48	0.128	0.079	0.008	0.026	0.087	68.57	6.82	24.61	75.39	10.1
26	QLD2J-39	Sandstone	293	0.089	0.066	0.008	0.003	0.074	83.27	10.52	6.21	93.79	7.9
Minimum									32.60	3.27	4.42	44.68	1.7
Maximum									89.00	27.64	55.32	95.58	18.9
Average									62.76	16.11	21.57	78.43	5.8

Sat saturated, *Aro* aromatic hydrocarbons, *NSO* nitrogen, sulfur, and oxygen, *HCs* hydrocarbon fractions (saturated + aromatic), *Sat/Aro* ratio of saturated hydrocarbons to aromatic hydrocarbons

toring the total inorganic carbon mass chromatograms (TIC) and m/z 85 ion mass chromatograms (see Fig. 6 and Table 2). The peak assignments used for biomarker parameters are listed in “Appendix.” In general, the n -alkane distributions of the non-biodegraded samples consist of a full suite of saturated hydrocarbons of n -alkanes (between C_{13} and C_{35}) and isoprenoids (Peters and Moldowan 1993; Peters et al. 2004). The presence of n -alkanes (extending beyond C_{31}) in the analyzed samples suggests that the studied oil possessed no or very low levels of biodegradation (e.g., Peters and Moldowan 1993; Peters et al. 2004; Wentzel et al. 2007). The values of Pr/Ph range from 1.07 to 2.89 (average 2.06), whereas those of Pr/ nC_{17} and Ph/ nC_{18} range from 0.25 to 2.19 (average 0.68) and 0.10

**Figure 5.** Ternary diagram of the extracted oil sand samples showing the compositions of the extracted oil.

to 1.16 (average 0.39), respectively. On the other hand, carbon preference index (CPI) values that are higher or lower (i.e., odd or even preferences, respectively) than 1.10 suggest that a sample is thermally immature (Peters and Moldowan 1993; Makeen et al. 2015a). The corresponding CPI values of the samples studied here range from 0.96 to 1.13 (average 1.06) (Table 2).

Terpane and Steroid Compositions

The terpane and steroid distributions of the studied saturated hydrocarbons were analyzed. Various biomarker maturity- and source-dependent parameters, such as tricyclic terpanes, hopane, homohopane, regular steranes, and diasterane, were determined based on the m/z 191 and m/z 217 mass chromatograms (Fig. 7). The identified peaks are shown in “Appendix.”

C_{30} hopane and C_{29} norhopane, T_s ($18\alpha(H)$ -trisorhopane), T_m ($17\alpha(H)$ -trisorhopane), and gammacerane were recorded from the m/z 191 mass chromatograms of the saturated hydrocarbon fractions of all studied samples (e.g., Fig. 7). The m/z 191 mass fragmentograms of the saturated hydrocarbon fractions of all oil samples show high proportions of C_{29} norhopane relative to C_{30} hopane (average 0.45), indicating a clay-rich source for the studied oil extracted from the oil sands (Peters et al. 2004). The ratio of T_s [$18\alpha(H)$ -trisorhopane] to T_m [$17\alpha(H)$ -trisorhopane] varies with maturation, the type of organic matter, and lithology (Moldowan et al. 1986). During the epigenesis stage, because the molecular energy of T_s is higher than that of T_m (i.e., 18.4 kJ/mol), the stability of T_s is higher than that of T_m . With increasing maturity, the value of $T_s/(T_s + T_m)$ gradually increases (Seifert and Moldowan 1978). The $T_s/(T_s + T_m)$ values of the extracted oil range from 0.50 to 0.73, with an average value of 0.56, thus reflecting the high maturity of these oil sands. Gammacerane is a reliable indicator for detecting the environmental conditions of the original source input. Abundant gammacerane generally indicates that sediments were deposited in saline water, which is often related to stratification of the water column (Damsté et al. 1995).

The m/z 217 mass fragmentograms of all analyzed samples display the relative abundance of steranes, including the C_{27} , C_{28} , and C_{29} regular steranes, as well as the ratios of C_{27}/C_{29} regular

sterane, diasterane/sterane, and sterane/hopane (Table 2). The relative C_{27} – C_{28} – C_{29} relationships of the analyzed samples are calculated, and the results show a high proportion of C_{29} sterane (ranging from 40.51 to 50.00%) compared to C_{28} sterane (ranging from 12.62 to 21.43%) and C_{27} sterane (ranging from 28.57 to 44.09%) (Table 2 and Fig. 8).

Aromatic Biomarkers and Tetracyclic Polyprenoids (TPP)

Numerous aromatic biomarker parameters, such as dibenzothiophene and phenanthrene, can be used to provide valuable information about the maturity range of organic matter (Radke et al. 1982; Makeen et al. 2015c). Information about source rock characteristics can also be obtained based on monoaromatic steroids (Moldowan et al. 1986). The aromatic biomarker ratios calculated in this study are presented in Table 3 and are based on peak heights and relative abundances.

The methylphenanthrene index (MPI) is one of the most widely used aromatic maturity parameters (Radke et al. 1982). Aromatic biomarker parameters have been derived for the distribution of methylphenanthrene and phenanthrene isomers in type III organic matter, including coals (Radke et al. 1986). The MPI values calculated here are based on the formula proposed by Radke et al. (1982): $MPI = 1.5 \frac{(2-MP + 3-MP)}{(P + 1-MP + 9-MP)}$, where P is the peak area of phenanthrene and 3-MP, 2-MP, 9-MP, and 1-MP are the peak areas of 3-, 2-, 9-, and 1-methylphenanthrenes, respectively (Fig. 9a and b). The results found using this formula indicate that all of the analyzed samples have MPI values ranging from 0.52 to 1.02 (Table 3), indicating that the studied samples are in the early mature to mature stages of petroleum generation.

Methyldibenzothiophenes are another type of mature aromatic hydrocarbon component that can be identified using m/z 198 because they respond more effectively than phenanthrenes in the medium to low maturity stages (Peters and Moldowan 1993). Dzou et al. (1995) examined a set of coals and oil and found a constant amount of 1-methyldibenzothiophene (1-MDBT) within a wide maturity range and an increase in 4-methyldibenzothiophene (4-MDBT) with increasing maturity. The relative increase in 4-MDBT during maturation is attributed to its higher thermostability (Radke et al. 1986).

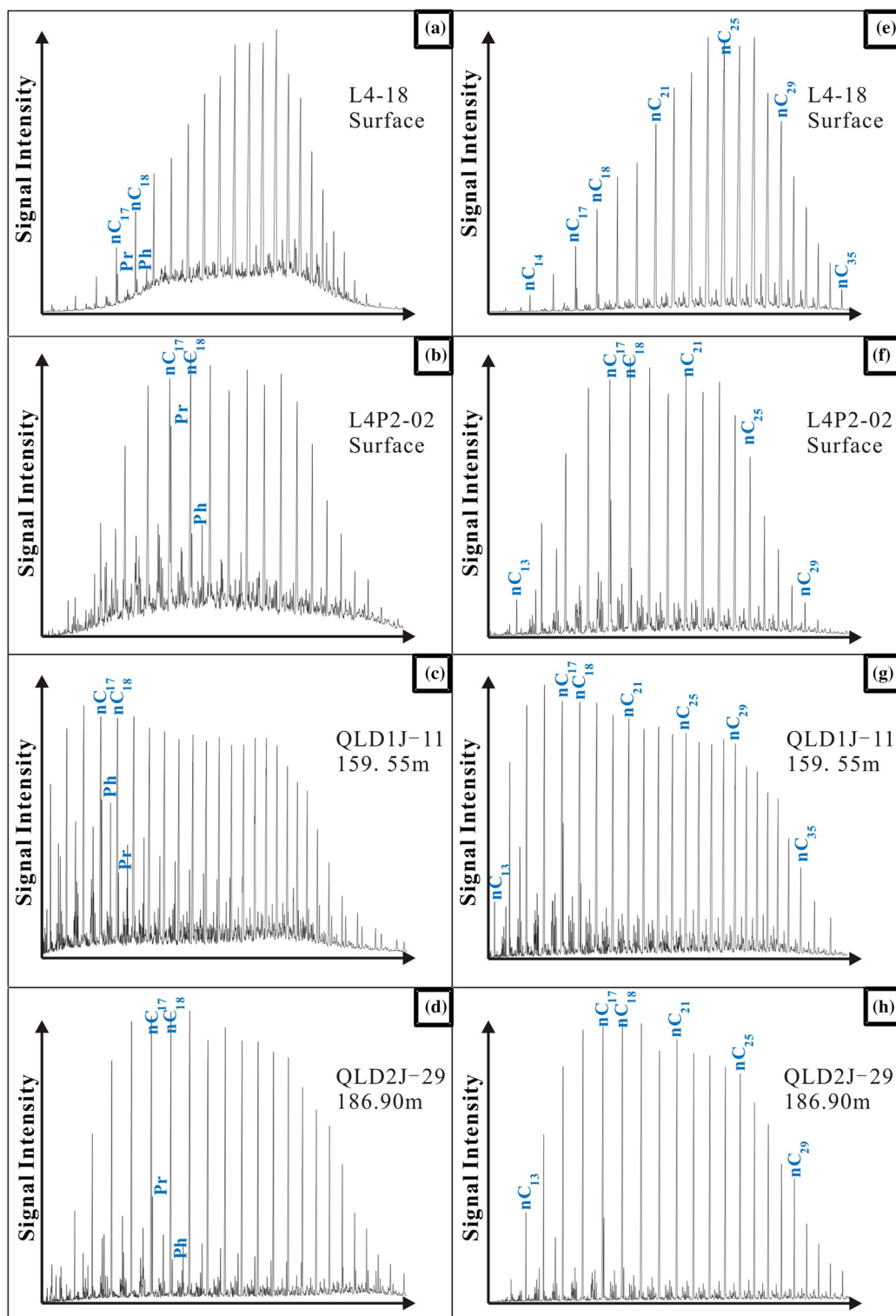


Figure 6. (a–d): total inorganic carbon mass chromatograms (TIC) and (e–h): m/z 85 ion chromatograms of the saturated hydrocarbons of the extracted oil.

Table 2. Results of the analyses of saturated biomarkers from extracted oil sands

No.	Sample ID	Normal alkanes and isoprenoids				Triterpanes and terpanes (<i>m/z</i> 191)						
		Pr/Ph	Pr/ <i>n</i> C ₁₇	Ph/ <i>n</i> C ₁₈	CPI	C ₃₂ 22 <i>S</i> / (22 <i>S</i> + 22 <i>R</i>)	Hopane terpanes					Tricyclic terpanes C ₂₆ <i>T</i> / C ₂₅ <i>T</i>
							C ₂₉ / C ₃₀	C _{31<i>R</i>} / C ₃₀	G/ C ₃₀	C ₃₀ <i>M</i> / C ₃₀ <i>H</i>	T _s / T _s + T _m	
1	L4-02	1.12	0.25	0.31	1.13	0.62	0.70	0.19	0.07	0.09	0.73	1.62
2	L4-05	1.65	1.50	0.79	1.11	0.58	0.46	0.12	0.05	0.14	0.50	1.38
3	L4-07	1.07	0.61	0.71	1.03	0.59	0.59	0.17	0.05	0.11	0.52	1.53
4	L4-10	2.08	0.51	0.57	0.98	0.60	0.50	0.12	0.05	0.13	0.59	1.86
5	L4-18	1.33	0.38	0.18	1.12	0.62	0.48	0.18	0.05	0.09	0.60	2.11
6	L4-21	1.52	0.96	0.26	1.09	0.59	0.41	0.11	0.05	0.14	0.55	1.39
7	L4P2-01	1.38	0.84	0.51	1.04	0.58	0.59	0.18	0.04	0.09	0.50	1.24
8	L4P2-02	2.08	0.53	0.24	1.06	0.64	0.52	0.15	0.06	0.12	0.57	1.63
9	L4-P3-02	1.75	1.50	0.86	0.96	0.63	0.52	0.21	0.05	0.07	0.71	1.22
10	L4-P3-04	1.60	0.35	0.20	1.11	0.63	0.47	0.23	0.07	0.11	0.59	1.33
11	LH4H-01	1.91	0.79	0.34	1.04	0.58	0.38	0.12	0.05	0.14	0.53	1.76
12	LH4H-02	1.75	0.29	0.12	1.12	0.59	0.45	0.20	0.07	0.11	0.65	1.57
13	LH4H-04	2.43	0.61	0.24	1.06	0.58	0.38	0.11	0.05	0.13	0.54	1.29
14	QLD1J-11	2.02	0.64	0.32	1.04	0.57	0.39	0.14	0.05	0.13	0.53	1.74
15	QLD1J-12	2.48	0.66	0.25	1.05	0.59	0.40	0.14	0.05	0.11	0.52	1.77
16	QLD1J-13	2.50	0.41	0.16	1.05	0.58	0.38	0.14	0.04	0.12	0.51	1.55
17	QLD1J-14	2.29	0.50	0.22	1.04	0.59	0.40	0.14	0.05	0.12	0.54	1.42
18	QLD2J-1	2.85	0.94	0.36	1.05	0.58	0.40	0.14	0.04	0.13	0.53	1.20
19	QLD2J-2	2.36	0.62	0.41	1.01	0.58	0.40	0.14	0.05	0.13	0.51	1.34
20	QLD2J-4	2.09	0.61	0.59	1.03	0.61	0.43	0.14	0.05	0.13	0.51	1.58
21	QLD2J-11	2.89	0.29	0.10	1.10	0.58	0.38	0.11	0.06	0.14	0.52	1.28
22	QLD2J-16	2.08	0.57	0.81	1.03	0.59	0.43	0.15	0.04	0.13	0.52	1.70
23	QLD2J-18	1.89	2.19	1.16	1.04	0.62	0.39	0.15	0.05	0.14	0.71	1.33
24	QLD2J-29	2.57	0.50	0.19	1.06	0.57	0.40	0.12	0.06	0.14	0.51	1.48
25	QLD2J-35	2.85	0.36	0.13	1.04	0.60	0.39	0.12	0.06	0.15	0.53	1.16
26	QLD2J-39	2.88	0.27	0.10	1.10	0.59	0.42	0.11	0.05	0.15	0.53	1.94
Minimum		1.07	0.25	0.10	0.96	0.57	0.38	0.11	0.04	0.07	0.50	1.16
Maximum		2.89	2.19	1.16	1.13	0.64	0.70	0.23	0.07	0.15	0.73	2.11
Average		2.06	0.68	0.39	1.06	0.60	0.45	0.15	0.05	0.12	0.56	1.52

Therefore, within a group of related oil or source rocks (aromatic hydrocarbons), the 4-MDBT/1-MDBT ratio commonly increases with increasing maturity (e.g., Dzou et al. 1995). Based on this classification, all of the analyzed samples display a high abundance of 4-methyldibenzothiophene (Table 3).

The dibenzothiophene/phenanthrene (DBT/P) ratios of the studied samples are shown in Table 3. DBT/P was measured (based on relative abundances) from the GC-MS analysis of the aromatic fraction using the *m/z* 184 and 178 ion chromatograms for DBT and P, respectively (e.g., Hughes 1995). The ratio of DBT to P is an indicator of source rock lithology. To identify biomarkers in detail, GC-MS/MS analyses were performed (Table 3) on tetracyclic polyprenoids (TPP) to find evidence of semimetal conditions.

Elemental Analysis

The composition of inorganic constituents, such as major and trace elements, is a good indicator of the provenance, redox conditions during sedimentation, effects of the preservation of organic matter, water salinity, and paleoclimate (Gromet et al. 1984). Trace element compositions can be determined using ICP-MS (Eggins et al. 1998). Trace elements in sediments, such as V, Ni, U, Cr, and Fe, are indicators of the paleo-redox conditions of sedimentary basins (e.g., Fu and Mazza 2011; Hakimi et al. 2015). Similarly, sedimentary environments can be classified based on the concentrations of trace elements such as Ba, Ga, Rb, and Sr (Reimann et al. 1998).

The extracted oil contains metallic elements, such as nickel (Ni) and vanadium (V) (Table 4).

Table 2. continued

No.	Sample ID	Steranes and diasteranes (<i>m/z</i> 217)							Sterane/hopane
		$C_{29}20S/$ (20S + 20R)	$C_{29}bb/$ (bb + aa)	Regular steranes			C_{27}/C_{29}	C_{27} Dia./ (Dia + Reg)	
				(%)					
				C_{27}	C_{28}	C_{29}			
1	L4-02	0.61	0.46	41.86	16.28	41.86	1.00	0.73	0.18
2	L4-05	0.46	0.44	38.02	17.43	44.55	0.85	0.47	0.04
3	L4-07	0.58	0.44	31.82	20.45	47.73	0.67	0.66	0.19
4	L4-10	0.47	0.45	36.83	16.21	46.95	0.78	0.60	0.09
5	L4-18	0.51	0.48	32.00	18.00	50.00	0.64	0.58	0.21
6	L4-21	0.45	0.45	41.36	14.07	44.57	0.93	0.56	0.16
7	L4P2-01	0.56	0.45	33.33	19.05	47.62	0.70	0.56	0.23
8	L4P2-02	0.53	0.46	28.57	21.43	50.00	0.57	0.54	0.18
9	L4-P3-02	0.52	0.44	40.00	13.33	46.67	0.86	0.61	0.15
10	L4-P3-04	0.53	0.46	38.96	19.48	41.56	0.94	0.56	0.17
11	LH4H-01	0.46	0.44	39.03	13.83	47.13	0.83	0.57	0.12
12	LH4H-02	0.51	0.48	37.14	17.14	45.71	0.81	0.61	0.16
13	LH4H-04	0.46	0.45	40.52	14.12	45.35	0.89	0.56	0.13
14	QLD1J-11	0.54	0.48	43.56	14.41	42.03	1.04	0.55	0.13
15	QLD1J-12	0.56	0.45	41.29	15.27	43.44	0.95	0.57	0.14
16	QLD1J-13	0.53	0.46	41.75	15.09	43.16	0.97	0.55	0.13
17	QLD1J-14	0.55	0.46	42.98	14.89	42.14	1.02	0.54	0.13
18	QLD2J-1	0.51	0.44	41.14	18.35	40.51	1.02	0.57	0.14
19	QLD2J-2	0.55	0.46	42.70	14.10	43.20	0.99	0.56	0.13
20	QLD2J-4	0.55	0.45	40.11	16.66	43.23	0.93	0.57	0.13
21	QLD2J-11	0.43	0.42	37.76	14.25	48.00	0.79	0.36	0.12
22	QLD2J-16	0.54	0.47	43.18	13.94	42.87	1.01	0.55	0.13
23	QLD2J-18	0.55	0.47	44.09	14.32	41.59	1.06	0.52	0.14
24	QLD2J-29	0.47	0.47	41.95	12.62	45.43	0.92	0.56	0.13
25	QLD2J-35	0.47	0.44	40.78	13.41	45.81	0.89	0.58	0.13
26	QLD2J-39	0.46	0.45	40.89	15.21	43.90	0.93	0.53	0.19
Minimum		0.43	0.42	28.57	12.62	40.51	0.57	0.36	0.04
Maximum		0.61	0.48	44.09	21.43	50.00	1.06	0.73	0.23
Average		0.51	0.45	39.29	15.90	44.81	0.88	0.56	0.15

Pr, pristane; *Ph*, phytane; *CPI*, carbon preference index ($2[C_{23} + C_{25} + C_{27} + C_{29}]/[C_{22} + 2\{C_{24} + C_{26} + C_{28}\} + C_{30}]$); C_{29}/C_{30} , C_{29} norhopane/ C_{30} hopane; $C_{30} M/C_{30} H$, C_{30} moretane/ C_{30} hopane; G/C_{30} , gammacerane/ C_{30} hopane; $C_{31}R/C_{30}$, C_{31} regular homohopane/ C_{30} hopane; diasterane/sterane ratio, C_{29} diasteranes/ C_{29} regular steranes; sterane/hopane ratio, C_{29} regular sterane/ C_{30} hopane

Although the V and Ni concentrations in oil depend on their degree of oil alteration, e.g., their biodegradation and maturity, the concentrations of V and Ni in oil can also provide insights into the depositional environment conditions of their potential source rocks (Lewan and Maynard 1982; Barwise 1990).

Py-GC Data

The Py-GC technique was developed in the late 1960s to study organic matter structural moieties, such as aromaticity, alkyl chain distribution, and organic sulfur structures (Chiavari and Galletti

1992). This method has been commonly used to provide information about the kerogen composition and type of hydrocarbons generated during the maturation process. According to Larter and Douglas (1980), different types of kerogens can be classified based on the carbon number distribution of *n*-alkanes. The amounts of type I pyrogram *n*-alkane/*n*-alkene are abundant in the C_{20} – C_{30} range, whereas the type II pyrograms always consist of fewer than 20 atoms of carbon in these compounds (e.g., Larter and Douglas 1980). Selected chromatograms of the asphaltenes precipitated from the studied oil sands are shown in Figure 10. The distribution of these compounds is characterized by *n*-alkane/*n*-alkene doublets extending beyond C_{30} .

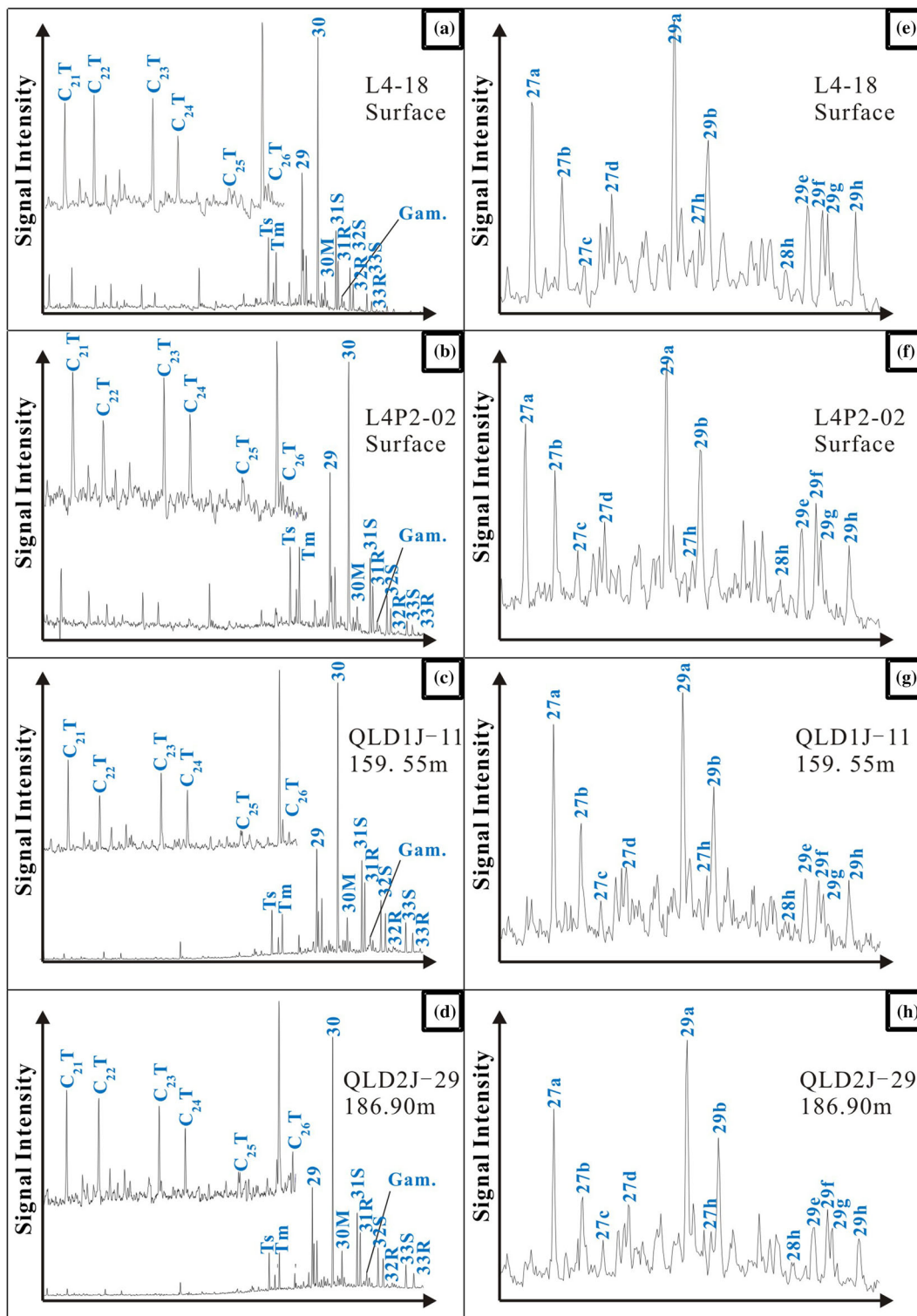


Figure 7. (a–d): m/z 191 ion chromatograms of the saturated hydrocarbons of the extracted oil; (e–h): m/z 217 ion chromatograms of the saturated hydrocarbons of the extracted oil.

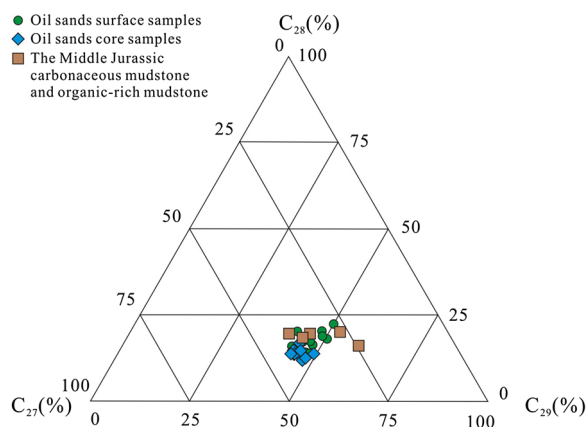


Figure 8. Ternary diagram of the C_{27} – C_{28} – C_{29} steranes for the oil obtained from oil sands and the Middle Jurassic carbonaceous mudstones and organic-rich mudstone source rocks of the Dameigou Formation, indicating the relationships between these sterane compositions (after Qin et al. 2018).

Aromatic compounds such as X -($m + p$)-xylenes and S -2,3-dimethylthiophene, along with nC_9 - n -alkanes, were also identified (Table 5).

DISCUSSION

Oil–Source Rock Correlation

An oil–source rock correlation involves performing the geochemical comparison of oil with extracts from potential source rocks to determine whether a genetic relationship exists. These correlation analyses are accomplished by comparing elemental and molecular parameters using techniques such as GC and GC–MS (Peters et al. 2004; Makeen et al. 2015d; Mohialdeen et al. 2015). The main objective of the correlation analysis in this study is to

Table 3. Results of the analyses of the aromatic biomarkers from extracted oil sands

No.	Sample ID	MPI	4-MDBT/1-MDBT	DBT/Phen	TPP ratio
1	L4-02	0.83	1.80	0.10	0.75
2	L4-05	0.66	1.11	0.02	–
3	L4-07	0.79	2.30	0.20	0.70
4	L4-10	0.57	1.01	0.05	–
5	L4-18	0.59	1.70	0.09	0.67
6	L4-21	0.64	1.58	0.02	–
7	L4P2-01	0.79	2.50	0.10	0.70
8	L4P2-02	0.92	1.90	0.20	0.70
9	L4-P3-02	0.74	1.90	0.01	–
10	L4-P3-04	0.52	2.70	0.20	0.66
11	LH4H-01	0.67	2.38	0.02	–
12	LH4H-02	0.74	2.90	0.08	–
13	LH4H-04	0.84	2.40	0.14	–
14	QLD1J-11	0.85	2.03	0.19	–
15	QLD1J-12	0.91	1.91	0.18	–
16	QLD1J-13	0.95	1.79	0.22	–
17	QLD1J-14	0.92	2.04	0.17	–
18	QLD2J-1	0.96	1.84	0.14	–
19	QLD2J-2	0.90	1.95	0.12	–
20	QLD2J-4	1.02	1.63	0.04	–
21	QLD2J-11	0.82	2.23	0.20	–
22	QLD2J-16	0.86	2.03	0.19	–
23	QLD2J-18	0.86	1.92	0.18	–
24	QLD2J-29	0.83	2.43	0.22	–
25	QLD2J-35	0.83	2.23	0.20	–
26	QLD2J-39	0.85	2.20	0.20	–
Minimum		0.52	1.01	0.01	0.66
Maximum		1.02	2.90	0.22	0.75
Average		0.80	2.02	0.13	0.70

MPI, $1.5(2\text{-MP} + 3\text{-MP})/(P + 1\text{-MP} + 9\text{-MP})$, where MP, methylphenanthrene; 1-MDBT, 1-methyldibenzothiophene; 4-MDBT, 4-methyldibenzothiophene; DBT/Phen, dibenzothiophene/phenanthrene; TPP, tetracyclic polyprenoids (the structure of C_{30} tetracyclic polyprenoid) for selected samples

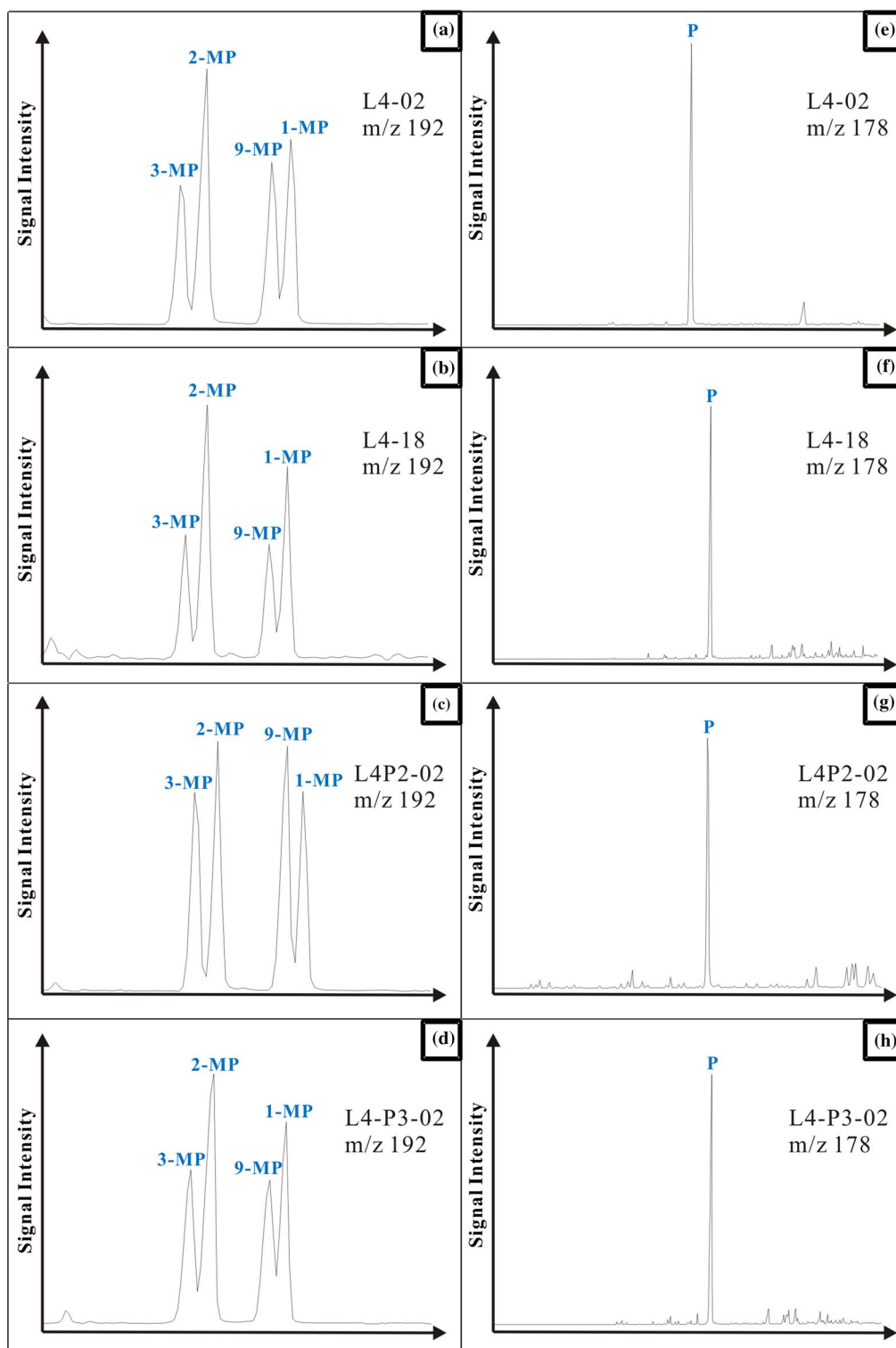


Figure 9. Chromatograms of the aromatic hydrocarbons in the extracted oil: (a-d) distribution of four methylphenanthrene isomers at m/z 192; (e-h) distribution of phenanthrene at m/z 178.

Table 4. Major and trace element (ppm) compositions of the analyzed samples

Sample ID	Major and trace elements (ppm)														
	AL	K	Ca	Ti	V	Cr	Fe	Ni	Ga	Sr	Ba	U	V/Ni	V/Cr	V/(V + Ni)
L4-02	546.1	12.83	293.9	20,290	4.79	6.04	769.5	2.47	4.06	28.9	21.48	6.72	1.94	0.79	0.66
L4-07	880.8	42.98	506.1	5614	4.4	23.51	1062	3.33	3.93	58.14	19.38	14.93	1.32	0.19	0.57
L4-18	1675	95.01	957.8	13,510	14.4	55.38	1770	6.47	8.48	195	102.5	75.44	2.23	0.26	0.69
L4P2-01	672.9	100.4	296.7	3567	3.87	3.12	292.5	1.84	3.88	37.73	18.97	7.83	2.10	1.24	0.68
L4P2-02	910.1	34.85	431.6	2624	3.93	2.24	274.5	0.86	3.82	25.28	16.48	6.8	4.57	1.75	0.82
L4-P3-02	1125	47.47	672.4	7642	7.1	11.8	734.8	1.92	4.93	78.46	37.61	13.43	3.70	0.60	0.79
L4-P3-04	763.2	27.05	251.5	3795	7.02	14.14	374.6	0.37	3.69	25.34	14.94	11.01	19.0	0.50	0.95
LH4H-02	1406	105.8	602.3	3664	48.09	49.85	1121	4.78	10.63	105.8	51.38	29.22	10.1	0.96	0.91
Average	997	58	502	7588	12	21	800	3	5	69	35	21	6	0.79	0.76

establish a genetic relationship (correlation) between the oil sands of the Oligocene Lower Ganchaigou Fm and the Middle Jurassic source rocks. Previous studies (Yang et al. 2004; Yin et al. 2008; Cao et al. 2009; Fu and Mazza 2011; Guo et al. 2018) interpreted the Middle Jurassic carbonaceous mudstones and organic-rich mudstones to be the major source rocks in the Northern Qaidam Basin. Cao et al. (2009) reported that the Lower and Middle Jurassic source rocks are believed to be the main source rocks in the Northern Qaidam Basin because they have relatively high total organic carbon (TOC) contents (4.0% and 5.0%, respectively).

Yang et al. (2004), Yin et al. (2008), Fu and Mazza (2011), and Guo et al. (2018) conducted detailed analyses of the organic geochemical characteristics of the Lower and Middle Jurassic source rocks of the Northern Qaidam Basin, including their origin and type of organic matter, thermal maturity, and environmental conditions. The Lower Jurassic sediments have a wider range of thermal maturities, ranging from relatively immature to highly mature, and they contain a mixture of Types II and III kerogens, while the Middle Jurassic sediments are generally immature to mature source rocks, with mainly Types I–II kerogens (Yin et al. 2008). Thus, Fu and Mazza (2011) believed that the Lower Jurassic sediments could generate commercial quantities of oil and gas, whereas the Middle Jurassic sediments may generate mainly oil due to their oil-prone kerogen type (Types I–II). In this study, the oil from the Oligocene Lower Ganchaigou Fm in the Northern Qaidam Basin and their asphaltene are similar to the Middle Jurassic sediments in terms of their kerogen types (Types I–II kerogens; see “Organic Matter Type” section) and maturity (see “Maturity of Organic Matter” sec-

tion), which suggests that the oil from the Oligocene Lower Ganchaigou Fm oil sand is mainly derived from Middle Jurassic source rocks.

Moreover, the Middle Jurassic source rocks contain more plants and minor aquatic algae than the Lower Jurassic source rocks; as a result, the $C_{27}R/C_{29}R$ regular sterane ratios of the Middle and Lower Jurassic rocks are less and greater than 1.0, respectively (Yang et al. 2004; Guo et al. 2018). The Middle Jurassic mudstones and carbonaceous mudstones are rich in C_{29} regular steranes, and the Lower Jurassic oil shales are comparatively richer in C_{27} regular steranes (Guo et al. 2018). The oil sands in the study area are characterized by low $C_{27}R/C_{29}R$ regular sterane ratios (i.e., high C_{29} regular steranes; see “Origin of Organic Matter” section), directly indicating that the oil studied here was generated from the Middle Jurassic carbonaceous mudstones and organic-rich mudstones. In addition, plots of $Pr/n-C_{17}$ vs. $Ph/n-C_{18}$ are widely used to classify oils and their related source rocks (Peters et al. 2005; Makeen et al. 2015d). The Pr/Ph ratios are low (< 0.8) in the Middle Jurassic oil shale and relatively high (1.9 and 2.8) in the carbonaceous mudstone and organic-rich mudstone samples (Guo et al. 2018). These relatively high Pr/Ph ratios suggest mixed organic matter deposited under sub-oxic to oxic conditions, which is in good agreement with the studied oil sands (see “Paleo-environmental Conditions” section).

Compositions of Extracted Oil

Together, the saturated and aromatic fractions comprise the petroleum-like hydrocarbon fractions. Hence, the sum of these two fractions is referred to

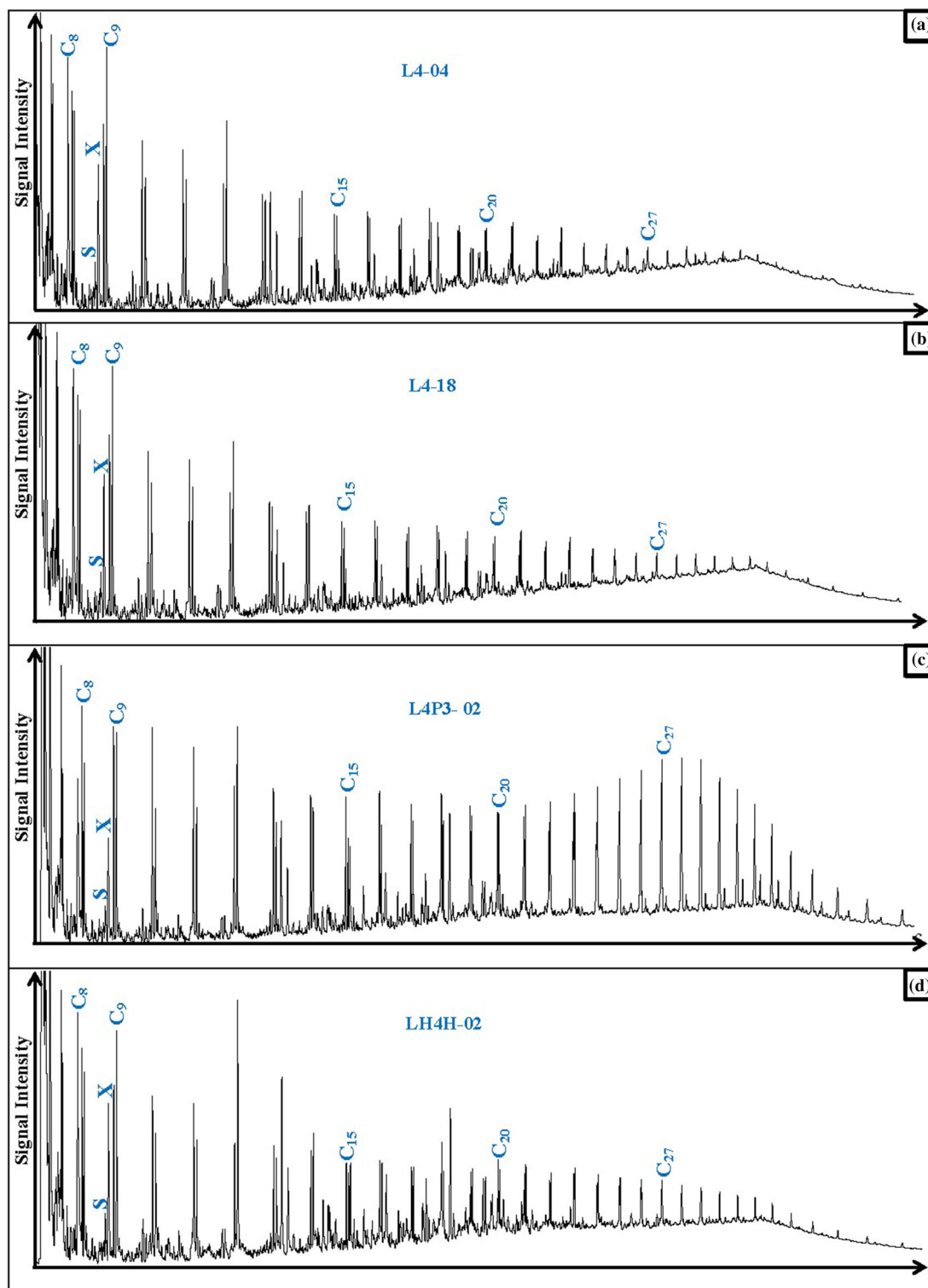
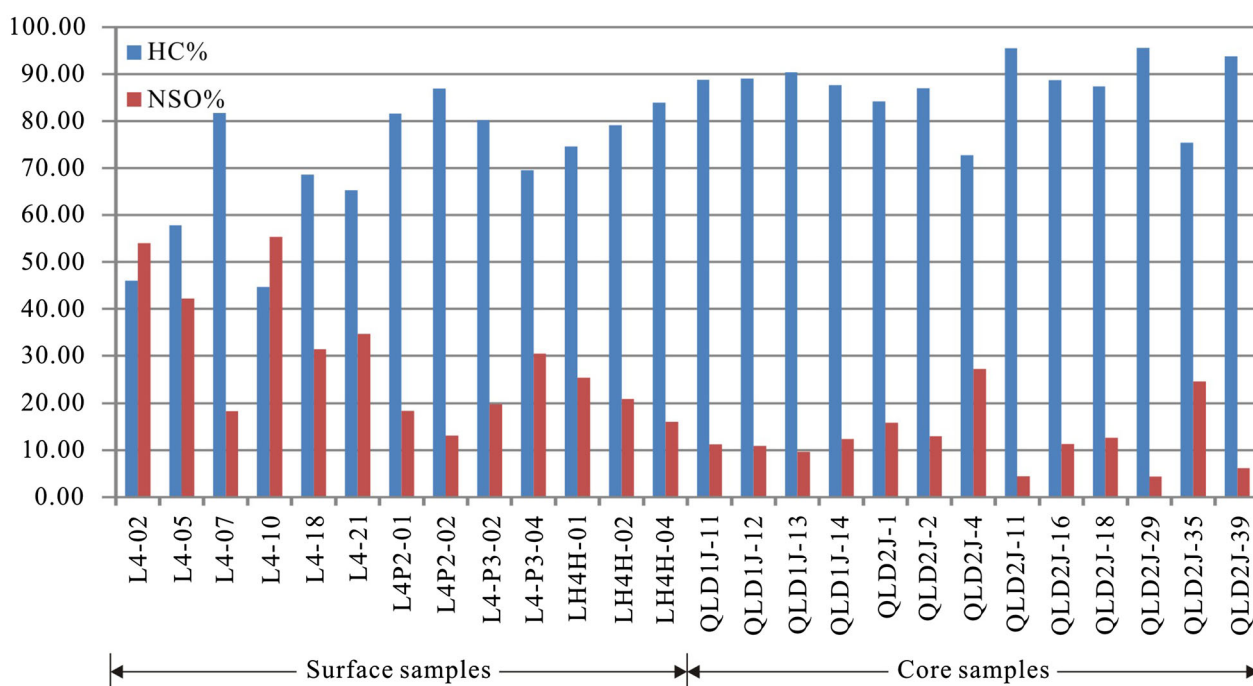


Figure 10. Pyrolysis–gas chromatography results obtained for the analyzed asphaltene samples showing doublet *n*-alkene/alkane peaks. *S*- and *O*-labeled peaks indicate 2,3-dimethylthiophene and ortho-xylene, respectively.

Table 5. Results of the Py-GC analyses of the extracted oil sands

No.	<i>X</i> -(<i>m</i> + <i>p</i>)-xylenes (%)	<i>S</i> -2,3-dimethylthiophene (%)	<i>n</i> C ₉ - <i>N</i> -alkanes (%)
L4-02	31	9	60
L4-07	32	8	60
L4-18	30	8	62
L4P2-01	36	8	56
L4-P3-02	28	6	66
L4-P3-04	40	6	54
LH4H-02	35	8	57
Minimum	28	6	54
Maximum	40	9	66
Average	33	8	59

**Figure 11.** Histogram showing the quantity of hydrocarbon (saturated + aromatic) and non-hydrocarbon (NSO) compounds derived from the extracted oil sands.

as hydrocarbons (HCs). The high proportions of hydrocarbons (average 78.43%) and relatively lower proportions of NSO (average 21.57%) (Table 1 and Fig. 11) suggest that the extracted oil samples are of high quality based on the classifications of Peters and Cassa (1994). This supposition is also supported by the high ratios of saturated to aromatic hydrocarbons (average 5.8). Compared with the surface

samples, the core samples are characterized by relatively higher hydrocarbon contents (Figs. 5 and 11).

Maturity of Organic Matter

Many parameters have been suggested and used to assess the thermal maturity of the Lower Gan-

chaigou Fm oil sands in the Northern Qaidam Basin. The studied oil sands are believed to be generated from thermally mature source rocks based on their biomarker maturity parameters, including C_{32} homohopane $22S/(22S + 22R)$, moretane/hopane, C_{29} sterane $20S/(20S + 20R)$, MPI, and MDBT, as well as their CPI values (e.g., Peters et al. 2004).

Table 2 shows that the $C_{29}\beta\beta/(\beta\beta + \alpha\alpha)$ and $20S/(20S + 20R)$ sterane values range from 0.42 to 0.48 and 0.43 to 0.61, respectively, thus indicating compositions that are typical of mature organic matter. According to Seifert and Moldowan (1978), the C_{32} $22S/22S + 22R$ homohopane ratio indicates that organic matter has barely entered the oil generation stage when its values fall within the range of 0.50–0.54, whereas ratios ranging from 0.54 to 0.62 indicate that the oil window has been reached

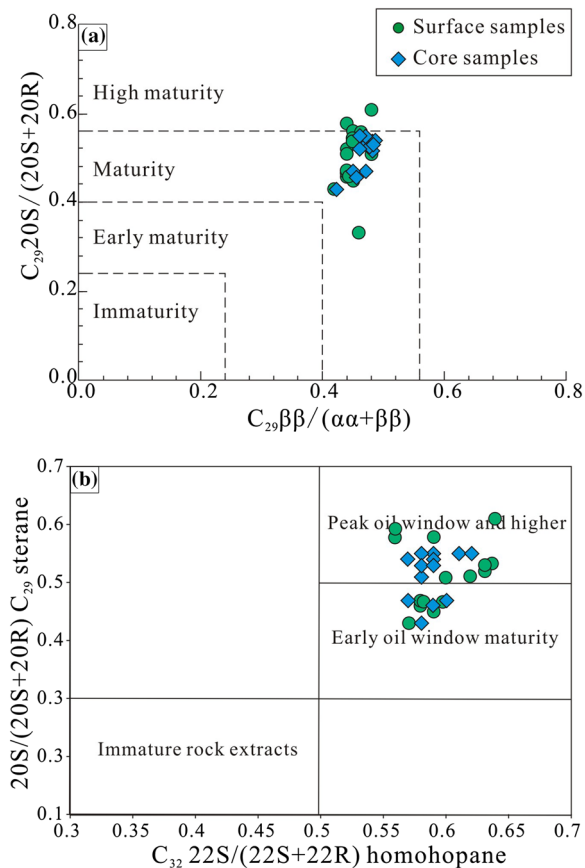


Figure 12. (a) $C_{29}\beta\beta/(\alpha\alpha + \beta\beta)$ vs. $C_{29}20S/(20S + 20R)$ values of extracted oil sands are indicative of maturity of oil sand oil in the study area; (b) cross-plot of $C_{29}20S/(20S + 20R)$ vs. $C_{32}22S/(22S + 22R)$ for the extracted oil sand samples showing that the organic matter in most of the studied oil sands entered the peak stage of the oil window (modified after Peters and Moldowan 1993).

(Fig. 12a). In the studied oil sands, the ratios of C_{32} hopane $22S/(22S + 22R)$ range from 0.57 to 0.64 (Table 2), suggesting that the source rock from which the extracted oil was generated had at least reached the early oil window (Fig. 12b). This supposition is also indicated by CPI values of ≈ 1 and supported by the MPI and 4-MDBT/1-MDBT ratio values as discussed previously (e.g., Wilhelms and Larter 2004). Furthermore, the value of the moretane/hopane ratio decreases with increasing thermal maturity; it is approximately 0.8 in immature bitumen and less than 0.15 in mature bitumen (Grantham 1986). The extracted oil from the Northern Qaidam Basin has an average moretane/hopane ratio value of 0.12, suggesting that the studied samples are derived from source rocks that have entered the oil window generation stage. This is further confirmed by their relatively high $T_s/(T_s + T_m)$ values (average 0.56). All of these data are consistent with the biomarker maturity parameters, vitrinite reflectance (approximately 0.6%), and T_{max} values of the Middle Jurassic carbonaceous mudstones and organic-rich mudstone source rocks of the Dameigou Fm previously reported by Yin et al. (2008) and Qin et al. (2018).

Paleo-environmental Conditions

The relative values of pristane (Pr) and phytane (Ph) are commonly used to evaluate the redox

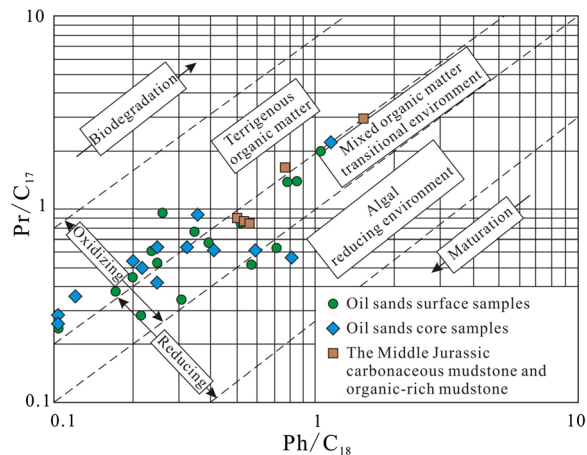


Figure 13. Relationship between the pristane/ nC_{17} index and phytane/ nC_{18} index for the investigated Lower Ganchaigou Fm oil sands and source rock extracts from the Middle Jurassic Dameigou Fm in the Northern Qaidam Basin, indicating the input of a mixed organic matter source (modified after Peters et al. 2004; Qin et al. 2018).

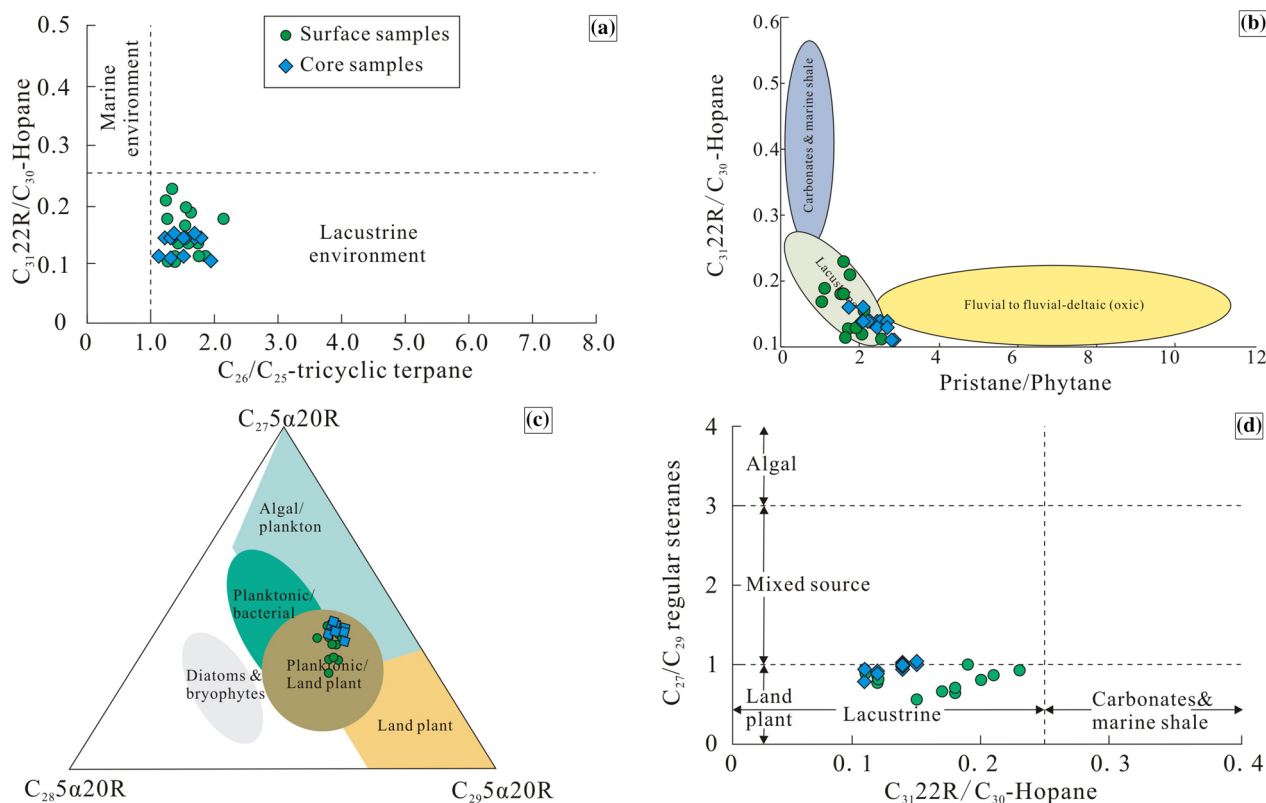


Figure 14. (a) $C_{31-22R}\text{-hopane}/C_{30}\text{-hopane}$ vs. $C_{26}/C_{25}\text{-tricyclic terpene}$, indicating a typical lacustrine environment for oil sands; (b) cross-plots of Pr/Ph vs. $C_{31-22R}/C_{30}\text{-hopane}$ ratios; (c) relationships between $\alpha\alpha\alpha C_{27}$ sterane 20R, $\alpha\alpha\alpha C_{28}$ sterane 20R, and $\alpha\alpha\alpha C_{29}$ sterane 20R, showing organic matter source input of the oil sand; and (d) cross-plot of C_{27}/C_{29} regular vs. $C_{31-22R}\text{-hopane}/C_{30}\text{-hopane}$, suggesting organic matter source input (modified after Peters et al. 2004). (a–c) are modified from Peters et al. (2004), Seifert and Moldowan (1978), and Peters et al. (2004), respectively.

conditions during sedimentation and diagenesis (Ten et al. 1987). Typically, Pr/Ph values ranging from 1.0 to 3.0 indicate sub-oxic depositional conditions, whereas high (> 3.0) and low values (< 0.6) of Pr/Ph indicate oxidizing and anoxic conditions, respectively (Waseda and Nishita 1998). Moreover, Pr/Ph values between 1 and 3 reflect oxidizing paleo-environmental conditions (Peters and Moldowan 1993). The oil extracted from the Northern Qaidam Basin has pristane/phytane (Pr/Ph) ratios ranging from 1.07 to 2.89 (Table 2), which further suggests that their organic matter was deposited under sub-oxic to oxic conditions (e.g., Makeen et al. 2015a, b). Additionally, their isoprenoid and n -alkane values were also calculated (Table 2). Therefore, a high contribution of mixed organic matter input is likely indicated by the relatively high values of Pr/ nC_{17} and Ph/ nC_{18} , which have mean values of 0.68 and 0.39, respectively (Peters et al. 2004; Qin et al. 2018). This contribution can be clearly seen on the plot of Pr/ nC_{17} vs. Ph/ nC_{18} ratios, in which the input of

mixed organic matter is associated with deposition within oxic to relatively anoxic depositional conditions (Fig. 13), and it is also suggested by the low values of gammacerane/ $\alpha\beta C_{30}$ hopane ratios (average 0.05) observed in all studied oil samples, which indicate a weak oxidation–reduction sedimentary environment. The mixed organic matter and sub-oxic to oxic paleo-environmental conditions indicated in this study are consistent with the carbonaceous mudstone and organic-rich mudstone source rocks of the Dameigou Fm previously reported by Qin et al. (2018) as shown in Figure 13.

Furthermore, low contents of uranium (U) (< 4 ppm) indicate an abundance of oxygen at the time of deposition, while high U contents (> 10 ppm) indicate anoxia (Galarraga et al. 2008; Pattan and Pearce 2009). The studied oil sand samples have relatively high U concentrations (6.72–75.44 ppm), indicating oxic to relatively anoxic depositional conditions. Additionally, iron (Fe_2O_3) and chromium (Cr) are also sensitive indicators of

paleo-redox conditions. Iron is easy to oxidize, and it is often associated with pyrite. The contents of iron (average 800 ppm) also indicate that oxic conditions prevailed during the deposition of these sediments. Furthermore, Cr is usually enriched in comparison with V under oxic conditions, and high values of the V/Cr ratio (> 4.25) indicate anoxic conditions and low values (< 2) suggest oxidizing conditions. The V/Cr ratios of the oil sand samples range from 0.19 to 1.75 (average 0.79), thus reflecting oxidizing conditions within a lacustrine environment.

The evidence for a predominantly lacustrine depositional environment is based on the observed C_{30} tetracyclic polyprenoid (TPP) ratios. High values of TPP ratios are observed in samples derived from lacustrine environments, and relatively low values are observed in samples derived from marine environments (Holba et al. 2003). The TPP ratios of the analyzed oil sand samples are relatively high (ranging from 0.66 to 0.75) (Table 3), indicating that the organic matter of the oil sands was deposited in a lacustrine environment (e.g., Silva et al. 2011), which is supported by the C_{26}/C_{25} tricyclic terpane ratios (Fig. 14a). The relative contents of $\alpha\beta C_{31-22R}$ -hopane and $\alpha\beta C_{30}$ hopane are also commonly used to distinguish between lacustrine and marine depositional environments (Peters et al. 2004). Generally, ratios of less than 0.2 indicate a lacustrine depositional environment, whereas higher ratios (more than 0.2) suggest a marine setting (Peters et al. 2004; Makeen et al. 2015a). The average ratio observed in the studied samples is 0.15, which therefore strongly argues for a lacustrine depositional environment (Fig. 14b), which is also consistent with their associated carbonaceous mudstones and mudstone source rocks of the Dameigou Fm.

Another paleo-environmental indicator is Sr/Ba (strontium/barium) (Langmuir and Melchior 1985). High Sr/Ba ratios result from high salinity, whereas low values suggest low salinity (Mohialdeen and Hakimi 2016; William et al. 2018). The studied oil sand samples show low Sr/Ba ratios (1.35–3.00 ppm), which is indicative of low-salinity depositional conditions. The V/Ni ratios and gammacerane index values also reflect low-salinity stratification during deposition.

Origin of Organic Matter

The sterane/hopane ratio is a measure of the eukaryotic vs. prokaryotic input to the source rocks (Peters et al. 2004). The mean value of the sterane/ho-

pane ratio observed here is 0.15, directly indicating a terrigenous sedimentary environment. Additionally, the origin of organic matter can also be evaluated using specific biomarker parameters, such as $\alpha\alpha C_{27}:C_{28}:C_{29}$ sterane 20R, pristane/ $n-C_{17}$ and phytane/ $n-C_{18}$, tricyclic terpane/ $\alpha\beta C_{30}$ hopane, and regular sterane/ $\alpha\beta C_{30}$ hopane (e.g., Huang and Meinschein 1979; Fu et al. 1990; De Grande et al. 1993; Peters et al. 2004). The relative abundances of regular C_{27} – C_{29} steranes are commonly used to evaluate the sources of precursors. C_{27} and C_{29} are indicative of algal and higher plant precursors, respectively (Huang and Meinschein 1979). In this study, the relative relationship between C_{27} – C_{28} – C_{29} suggests the dominance of higher plant organic matter (Fig. 14c) (e.g., Moldowan et al. 1986; Peters et al. 2017; Qin et al. 2018). This interpretation is also consistent with the plot of C_{27}/C_{29} regular sterane vs. C_{31-22R} -hopane/ C_{30} -hopane (Fig. 14d) and with the previously reported carbonaceous mudstone and organic-rich mudstone source rocks of the Dameigou Fm. The steranes diagram (Fig. 8) supports the relative correlation between these oil extracts and the Middle Jurassic carbonaceous mudstone and mudstone source rocks.

The source rock lithology can also be designated using biomarker parameters. A high C_{29} norhopane/ C_{30} hopane ratio suggests a carbonate-rich source for oil, whereas a low norhopane/ C_{30} hopane ratio indicates that the oil originates from clay-rich source rocks (Rabbani and Kamali 2005). In this study, the ratios of C_{29} norhopane to C_{30} hopane range from 0.38 to 0.70, indicating a clay-rich source for the oil studied here. Furthermore, the relationships between dibenzothio-phenone (DBT) and phenanthrene (P) are also indicators of source rock lithology (Hughes 1995). A DBT/P ratio of > 1 indicates a carbonate-type facies, while a DBT/P ratio of < 1 indicates a shale/mudstone-type lithology (e.g., Baumard et al. 1999). Based on this classification, all of the studied samples possess DBT/P ratios of < 1 , thus indicating a shale/mudstone lithology that is consistent with the Middle Jurassic source rocks of the Dameigou Fm. This directly suggests that the carbonaceous mudstone and organic-rich mudstone source rocks of the Dameigou Fm constitute the source rocks of the Lower Ganchaigou Fm oil sands in the study area.

Organic Matter Type

Asphaltene pyrolysis data can be used to provide information about the quality of the organic matter of source rocks (Makeen et al. 2015b). Type I

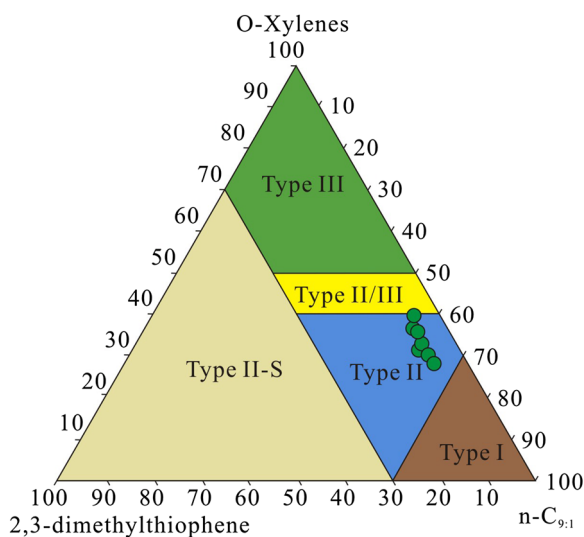


Figure 15. Ternary diagram of the compounds of 2,3-dimethylthiophene, o-xylene (1,2-dimethylbenzene), and *n*-non-1-ene (*n*-C_{9:1}) showing that the kerogen in the studied samples is Type II kerogen (adapted after Eglinton et al. 1990).

and Type II kerogens, which are commonly derived from marine and lacustrine organic matter sources, are capable of generating liquid hydrocarbons. Type III kerogen is mainly derived from woody material; therefore, it is susceptible to generating gas hydrocarbons. In contrast, Type IV kerogen is mainly composed of inert materials and has no hydrocarbon generation potential (Hakimi et al. 2011). In this study, a kerogen classification diagram was constructed based on the compounds of 2,3-dimethylthiophene, o-xylene (1,2-dimethylbenzene), and *n*-non-1-ene (*n*-C_{9:1}). The Py-GC analysis of the asphaltene from the analyzed samples suggests that the kerogen in all samples is Type II kerogen (Fig. 15), which is consistent with the Middle Jurassic carbonaceous mudstone and mudstone source rocks of the Dameigou Fm.

Aliphatic and aromatic hydrocarbons, as well as sulfur compounds, are the most important compounds that can be generated from pyrolysis analysis (Hakimi and Abdullah 2013; Makeen et al. 2015a). Xylene is the main aromatic compound that is commonly associated with type II organic matter, which is produced in amounts that closely elute *n*-hydrocarbons (Keym et al. 2006). In this study, ortho-xylene was present in relatively high amounts in all samples (Table 5 and Fig. 10), thus indicating a type II origin. On the other hand, thiophene sulfur compounds are another important group that forms

during pyrolysis analysis, and they normally do not occur in high abundances in natural oil or bitumen (Sinninghe and De 1990; Clegg et al. 1998). The occurrence of 2,3-dimethylthiophene in all analyzed samples is not high; therefore, it is directly related to the type of petroleum formed from its corresponding kerogen type in nature (e.g., Horsfield 1989).

Furthermore, the entire set of samples is tightly clustered (Fig. 10), and they are consistent with or similar to the liptinite-rich types of petroleum source rock. It should be noted that different trends of chromatograms cannot be observed for samples that seem to be composed of similar kerogen types (Keym et al. 2006), which suggests that the organic matter assemblages within the Qaidam Basin are very much homogeneous and thus may indicate a similar type of kerogen (Type II kerogen).

CONCLUSIONS

A suite of organic and inorganic geochemical evaluation techniques, including chemical composition analysis and analyses of biomarker parameters [e.g., MPI, MDBT, CPI C₂₉ norhopane/C₃₀ hopane, and dibenzothiophene (DBT)/phenanthrene (P)], were used to infer the organic matter type, thermal maturity, paleo-environmental conditions, and oil-source rock correlations using oil sands extracted from the Oligocene oil sands of the Lower Ganchaigou Fm in the Northern Qaidam Basin. The following conclusions were drawn.

1. The chemical composition analysis revealed that the oil samples are of high quality based on their high yield of hydrocarbon fractions (44.68–95.58%) and high ratio of saturated hydrocarbons to aromatic hydrocarbons.
2. The biomarker parameter analysis indicated that the thermal maturity conditions ranged from the early to peak oil window stages for the oil sands, which is generally consistent with the biomarker maturity parameters, vitrinite reflectance (approximately 0.6%), and T_{\max} values of the Middle Jurassic carbonaceous mudstones and organic-rich mudstones of the Dameigou Fm in the Northern Qaidam Basin.
3. The C₂₉ norhopane/C₃₀ hopane and dibenzothiophene (DBT)/phenanthrene (P) ratios indicate a shale/mudstone-type lithology.

4. Additionally, the observed relationships among the C_{27} – C_{28} – C_{29} ratios, other source input parameters, and paleo-environmental analysis reflect the dominance of plankton/land plant-sourced organic matter deposited in a lacustrine environment and preserved under sub-oxic to oxic conditions. This inference together with the high-yield hydrocarbon content and mudstone source lithology is consistent with and in support of the genetic relationship that has been previously reported for the carbonaceous mudstones and organic-rich mudstones of the Dameigou Fm.
5. The striking similarities between the structural kerogen type (Type II) of the studied asphaltenes and the previously published kerogen types of the carbonaceous mudstones and organic-rich mudstones of the Dameigou Fm imply that this formation could be the main source contributing to the reservoirs in the Northern Qaidam Basin. Hence, future hydrocarbon exploration processes in the Qaidam Basin should focus on areas that are known to receive a direct

charge from the Middle Jurassic source rocks of the Dameigou Fm, where the source rocks are likely to be more mature.

ACKNOWLEDGMENTS

This study was supported by Basic geological survey of oil Shale and oil Sands in Songliao, Qaidam and Erlian Basins (Grant No. DD20160188), China Geological Survey and China Scholarship Council (Grant No. 201701760617), and two key laboratories including Key Laboratory for Evolution of Past Life and Environment in Northeast Asia (Jilin University) and the Organic Geochemistry Laboratories of the Department of Geology, University of Malaya, Malaysia.

APPENDIX

See Table 6.

Table 6. Alkane hydrocarbon peaks of the saturated fraction obtained by GC–MS based on the m/z 191 (I) and m/z 217 (II) mass fragmentogram compound abbreviations

(I) Peak No.		
T_s	18 α (H),22,29,30-trisnorneohopane	T_s
T_m	17 α (H),22,29,30-trisnorhopane	T_m
29	17 α ,21 β (H)-norhopane	C ₂₉ hop
30	17 α ,21 β (H)-hopane	Hopane
30M	17 β ,21 α (H)-moretane	C ₃₀ Mor
29M	17 β (H),21 α (H)-30-norhopane (normoretane)	Normoretane
31S	17 α ,21 β (H)-homohopane (22S)	C ₃₁ (22S)
31R	17 α ,21 β (H)-homohopane (22R)	C ₃₁ (22R)
32S	17 α ,21 β (H)-homohopane (22S)	C ₃₂ (22S)
32R	17 α ,21 β (H)-homohopane (22R)	C ₃₂ (22R)
33S	17 α ,21 β (H)-homohopane (22S)	C ₃₃ (22S)
33R	17 α ,21 β (H)-homohopane (22R)	C ₃₃ (22R)
34S	17 α ,21 β (H)-homohopane (22S)	C ₃₄ (22S)
34R	17 α ,21 β (H)-homohopane (22R)	C ₃₄ (22R)
35S	17 α ,21 β (H)-homohopane (22S)	C ₃₅ (22S)
35R	17 α ,21 β (H)-homohopane (22R)	C ₃₅ (22R)
(II) Peak No.		
a	13 β ,17 α (H)-diasteranes 20S	Diasteranes
b	13 β ,17 α (H)-diasteranes 20R	Diasteranes
c	13 α ,17 β (H)-diasteranes 20S	Diasteranes
d	13 α ,17 β (H)-diasteranes 20R	Diasteranes
e	5 α ,14 α (H), 17 α (H)-steranes 20S	$\alpha\alpha\alpha$ 20S
f	5 α ,14 β (H), 17 β (H)-steranes 20R	$\alpha\beta\beta$ 20R
g	5 α ,14 β (H), 17 β (H)-steranes 20S	$\alpha\beta\beta$ 20S
h	5 α ,14 α (H), 17 α (H)-steranes 20R	$\alpha\alpha\alpha$ 20R

REFERENCES

- Adegoke, H. I., AmooAdekola, F., Fatoki, O. S., & Ximba, B. J. (2014). Adsorption of Cr(VI) on synthetic hematite (α -Fe₂O₃) nanoparticles of different morphologies. *Korean Journal of Chemical Engineering*, 31(1), 142–154.
- Bao, J., Wang, Y., Song, C., Feng, Y., Hu, C., Zhong, S., et al. (2017). Cenozoic sediment flux in the Qaidam Basin, northern Tibetan Plateau, and implications with regional tectonics and climate. *Global and Planetary Change*, 155, 56–69.
- Barwise, A. J. G. (1990). Role of nickel and vanadium in petroleum classification. *Energy & Fuels*, 4(6), 647–652.
- Baumard, P., Budzinski, H., Garrigues, P., Dizer, H., & Hansen, P. D. (1999). Polycyclic aromatic hydrocarbons in recent sediments and mussels (*Mytilus edulis*) from the Western Baltic Sea: Occurrence, bioavailability and seasonal variations. *Marine Environmental Research*, 47(1), 17–47.
- Cao, J., Bian, L., Hu, K., Liu, Y., Wang, L., Yang, S., et al. (2009). Benthic macro red alga: A new possible bio-precursor of Jurassic mudstone source rocks in the northern Qaidam Basin, northwestern China. *Science in China, Series D: Earth Sciences*, 52(5), 647–654.
- CAPP (Canadian Association of Petroleum Producers). (2017). *Crude oil forecast, markets and transportation*. <http://www.capp.ca/publications-and-statistics/publications/303440>. Accessed 5 December 2017.
- Chiavari, G., & Galletti, G. C. (1992). Pyrolysis—gas chromatography/mass spectrometry of amino acids. *Journal of Analytical and Applied Pyrolysis*, 24(2), 123–137.
- Clegg, H., Horsfield, B., Wilkes, H., Damsté, J., & Koopmans, M. (1998). Effect of artificial maturation on carbazole distributions, as revealed by the hydrous pyrolysis of an organic-sulphur-rich source rock (Ghareb Formation, Jordan). *Organic Geochemistry*, 29(8), 1953–1960.
- Damsté, J. S. S., Kenig, F., Koopmans, M. P., Köster, J., Schouten, S., Hayes, J. M., et al. (1995). Evidence for gammacerane as an indicator of water column stratification. *Geochimica et Cosmochimica Acta*, 59(9), 1895–1900.
- De Grande, S. M. B., Neto, F. A., & Mello, M. R. (1993). Extended tricyclic terpanes in sediments and petroleum. *Organic Geochemistry*, 20(7), 1039–1047.
- Du, D. D., Zhang, C. J., Mughal, M. S., Wang, X. Y., Blaise, D., Gao, J. P., et al. (2018). Detrital apatite fission track constraints on Cenozoic tectonic evolution of the northeastern Qinghai-Tibet Plateau, China: Evidence from Cenozoic strata in Lulehe section, Northern Qaidam Basin. *Journal of Mountain Science*, 15(3), 532–547.
- Duan, Y., Zheng, C., Wang, Z., Wu, B., Wang, C., Zhang, H., et al. (2006). Biomarker geochemistry of crude oils from the Qaidam Basin, NW China. *Journal of Petroleum Geology*, 29(2), 175–188.
- Dzou, L. I. P., Noble, R. A., & Senftle, J. T. (1995). Maturation effects on absolute biomarker concentration in a suite of coals and associated vitrinite concentrates. *Organic Geochemistry*, 23(7), 681–697.
- Eggins, S. M., Kinsley, L. P. J., & Shelley, J. M. G. (1998). Deposition and element fractionation processes during atmospheric pressure laser sampling for analysis by ICP-MS. *Applied Surface Science*, 127, 278–286.
- Eglinton, T. I., Damsté, J. S. S., Kohnen, M. E., & de Leeuw, J. W. (1990). Rapid estimation of the organic sulphur content of kerogens, coals and asphaltenes by pyrolysis—gas chromatography. *Fuel*, 69(11), 1394–1404.
- EIA. (2012). *Annual energy review 2011*. United States. <https://doi.org/10.2172/1212312>.
- Etxebarria, N., Zuloaga, O., Olivares, M., Bartolomé, L. J., & Navarro, P. (2009). Retention-time locked methods in gas chromatography. *Journal of Chromatography A*, 1216(10), 1624–1629.
- Feng, J., Cao, J., Hu, K., Peng, X., Chen, Y., Wang, Y., et al. (2013). Dissolution and its impacts on reservoir formation in moderately to deeply buried strata of mixed siliciclastic-carbonate sediments, northwestern Qaidam Basin, northwest China. *Marine and Petroleum Geology*, 39(1), 124–137.
- Fu, D., & Mazza, G. (2011). Optimization of processing conditions for the pretreatment of wheat straw using aqueous ionic liquid. *Bioresource Technology*, 102(17), 8003–8010.
- Fu, J., Sheng, G., Xu, J., Eglinton, G., Gowar, A., Jia, R., et al. (1990). Application of biological markers in the assessment of paleoenvironments of Chinese non-marine sediments. *Organic Geochemistry*, 16(4–6), 769–779.
- Galarraga, F., Reategui, K., Martínez, A., Martínez, M., Llamas, J. F., & Márquez, G. (2008). V/Ni ratio as a parameter in palaeoenvironmental characterisation of nonmature medium-crude oils from several Latin American basins. *Journal of Petroleum Science and Engineering*, 61(1), 9–14.
- Gao, Z., Zeng, L., & Niu, F. (2005). Unusually physical and chemical characteristics of oil sands from Qaidam basin, NW China. *Geochemical Journal*, 39(2), 121–130.
- Grantham, P. J. (1986). Sterane isomerisation and moretane/hopane ratios in crude oils derived from Tertiary source rocks. *Organic Geochemistry*, 9(6), 293–304.
- Gromet, L. P., Haskin, L. A., Korotev, R. L., & Dymek, R. F. (1984). The “North American shale composite”: Its compilation, major and trace element characteristics. *Geochimica et Cosmochimica Acta*, 48(12), 2469–2482.
- Guo, T., Ren, S., Luo, X., Bao, S., Wang, S., Zhou, Z., et al. (2018). Accumulation conditions and prospective areas of shale gas in the Middle Jurassic Dameigou Formation, northern Qaidam Basin, Northwest China. *Geological Journal*, 53(6), 2944–2954.
- Hakimi, M. H., & Abdullah, W. H. (2013). Organic geochemical characteristics and oil generating potential of the Upper Jurassic Safer shale sediments in the Marib-Shabowah Basin, western Yemen. *Organic Geochemistry*, 54, 115–124. <https://doi.org/10.1016/j.orggeochem.2012.10.003>.
- Hakimi, M. H., Mohialdeen, I. M., Abdullah, W. H., Wimbleton, W., Makeen, Y. M., & Mustapha, K. A. (2015). Biomarkers and inorganic geochemical elements of Late Jurassic-Early Cretaceous limestone sediments from Banik Village in the Kurdistan Region, Northern Iraq: Implications for origin of organic matter and depositional environment conditions. *Arabian Journal of Geosciences*, 8(11), 9407–9421.
- Hakimi, M., Selvanantham, T., Swinton, E., Padmore, R. F., Tong, Y., Kabbach, G., et al. (2011). Parkinson's disease-linked LRRK2 is expressed in circulating and tissue immune cells and upregulated following recognition of microbial structures. *Journal of Neural Transmission*, 118(5), 795–808.
- Holba, A. G., Dzou, L. I., Wood, G. D., Ellis, L., Adam, P., Schaeffer, P., et al. (2003). Application of tetracyclic polyprenoids as indicators of input from fresh-brackish water environments. *Organic Geochemistry*, 34(3), 441–469.
- Horsfield, B. (1989). Practical criteria for classifying kerogens: Some observations from pyrolysis-gas chromatography. *Geochimica et Cosmochimica Acta*, 53(4), 891–901.
- Huang, R., Kerry, N., Yang, L., & Mohamed, G. (2016). Characterization and distribution of metal and nonmetal elements in the Alberta oil sands region of Canada. *Chemosphere*, 147, 218–229.
- Huang, W. Y., & Meinschein, W. G. (1979). Sterols as ecological indicators. *Geochimica et Cosmochimica Acta*, 43(5), 739–745.
- Huang, D., Zhang, D., & Li, J. (1994). The origin of 4-methyl steranes and pregnanes from Tertiary strata in the Qaidam Basin, China. *Organic Geochemistry*, 22(2), 343–348.

- Hughes, T. J. (1995). Multiscale phenomena: Green's functions, the Dirichlet-to-Neumann formulation, subgrid scale models, bubbles and the origins of stabilized methods. *Computer Methods in Applied Mechanics and Engineering*, 127(1–4), 387–401.
- Ji, J., Zhang, K., Clift, P. D., Zhuang, G., Song, B., Ke, X., et al. (2017). High-resolution magnetostratigraphic study of the Paleogene–Neogene strata in the Northern Qaidam Basin: Implications for the growth of the Northeastern Tibetan Plateau. *Gondwana Research*, 46, 141–155.
- Keym, M., Dieckmann, V., Horsfield, B., Erdmann, M., Galimberti, R., Kua, L. C., et al. (2006). Source rock heterogeneity of the Upper Jurassic Draupne Formation, North Viking Graben, and its relevance to petroleum generation studies. *Organic Geochemistry*, 37(2), 220–243.
- Langmuir, D., & Melchior, D. (1985). The geochemistry of Ca, Sr, Ba and Ra sulfates in some deep brines from the Palo Duro Basin, Texas. *Geochimica et Cosmochimica Acta*, 49(11), 2423–2432.
- Larter, S. R., & Douglas, A. G. (1980). A pyrolysis-gas chromatographic method for kerogen typing. *Physics and Chemistry of the Earth*, 12, 579–583.
- Lewan, M. D., & Maynard, J. B. (1982). Factors controlling enrichment of vanadium and nickel in the bitumen of organic sedimentary rocks. *Geochimica et Cosmochimica Acta*, 46(12), 2547–2560.
- Li, Y., Li, X., Wang, Y., Yu, Q., Yingjie, L., Xiaoyuan, L., et al. (2015). Effects of composition and pore structure on the reservoir gas capacity of Carboniferous shale from Qaidam Basin, China. *Marine and Petroleum Geology*, 62, 44–57.
- Li, L., Wu, C., Fan, C., Li, J., & Zhang, C. (2017). Carbon and oxygen isotopic constraints on paleoclimate and paleoelevation of the southwestern Qaidam basin, northern Tibetan Plateau. *Geoscience Frontiers*, 8(5), 1175–1186.
- Lu, H., & Xiong, S. (2009). Magnetostratigraphy of the Dahonggou section, northern Qaidam Basin and its bearing on Cenozoic tectonic evolution of the Qilian Shan and Altyn Tagh Fault. *Earth and Planetary Science Letters*, 288(3–4), 539–550.
- Lu, Z., Zhang, J., & Mattinson, C. (2018). Tectonic erosion related to continental subduction: An example from the eastern North Qaidam Mountains, NW China. *Journal of Metamorphic Geology*, 36(5), 653–666.
- Makeen, Y. M., Abdullah, W. H., & Hakimi, M. H. (2015a). Biological markers and organic petrology study of organic matter in the Lower Cretaceous Abu Gabra sediments (Muglad Basin, Sudan): Origin, type and palaeoenvironmental conditions. *Arabian Journal of Geosciences*, 8(1), 489–506.
- Makeen, Y. M., Abdullah, W. H., & Hakimi, M. H. (2015b). The origin, type and preservation of organic matter of the Barremian Aptian organic-rich shales in the Muglad Basin, Southern Sudan, and their relation to paleoenvironmental and paleoclimate conditions. *Marine and Petroleum Geology*, 65(187–197), 2015.
- Makeen, Y. M., Abdullah, W. H., Hakimi, M. H., & Elhassan, O. M. (2015c). Organic geochemical characteristics of the Lower Cretaceous Abu Gabra Formation in the Great Moga oilfield, Muglad Basin, Sudan: Implications for depositional environment and oil-generation potential. *Journal of African Earth Sciences*, 103, 102–112.
- Makeen, Y. M., Abdullah, W. H., Hakimi, M. H., Hadad, Y. T., Mustapha, K. A., & Elhassan, O. M. A. (2015d). Geochemical characteristics of crude oils, their asphaltene and related organic matter source inputs from Fula oilfields in the Muglad Basin, Sudan. *Marine and Petroleum Geology*, 67, 816–828.
- Manzano, C., Muir, D., Kirk, J., Teixeira, C., Siu, M., Wang, X., et al. (2016). Temporal variation in the deposition of polycyclic aromatic compounds in snow in the Athabasca Oil Sands area of Alberta. *Environmental Monitoring and Assessment*, 188, 542.
- Mao, L., Xiao, A., Zhang, H., Wu, Z., Wang, L., Shen, Y., et al. (2016). Structural deformation pattern within the NW Qaidam Basin in the Cenozoic era and its tectonic implications. *Tectonophysics*, 687, 78–93.
- Marek, O., Mirjavad, G., Douglas, G., Liu, Q., & Thomas, H. (2013). Mineralogical and chemical composition of petrologic end members of Alberta oil sands. *Fuel*, 113, 148–157.
- Mei, M., Bissada, K., Malloy, T., Darnell, L., & Liu, Z. (2018). Origin of condensates and natural gases in the Almond Formation reservoirs in southwestern Wyoming, USA. *Organic Geochemistry*, 116, 35–50.
- Meng, Q. R., Hu, J. M., & Yang, F. Z. (2001). Timing and magnitude of displacement on the Altyn Tagh fault: Constraints from stratigraphic correlation of adjoining Tarim and Qaidam basins, NW China. *Terra Nova*, 13(2), 86–91.
- Métivier, F., Gaudemer, Y., Tapponnier, P., & Meyer, B. (1998). Northeastward growth of the Tibet plateau deduced from balanced reconstruction of two depositional areas: The Qaidam and Hexi Corridor basins, China. *Tectonics*, 17(6), 823–842.
- Mischke, S., Sun, Z., Herzsuh, U., Qiao, Z., & Sun, N. (2010). An ostracod-inferred large Middle Pleistocene freshwater lake in the presently hyper-arid Qaidam Basin (NW China). *Quaternary International*, 218(1–2), 74–85.
- Mohialdeen, I. M. J., & Hakimi, M. H. (2016). Geochemical characterisation of Tithonian–Berriasian Chia Gara organic-rich rocks in northern Iraq with an emphasis on organic matter enrichment and the relationship to the bioproductivity and anoxia conditions. *Journal of Asian Earth Sciences*, 116, 181–197.
- Mohialdeen, I. M. J., Hakimi, M. H., & Al-Beyati, F. M. (2015). Biomarker characteristics of some crude oils and oil–source rock correlation in the Kurdistan oilfields, Northern Iraq. *Arabian Journal of Geosciences*, 8, 507–523.
- Moldowan, J. M., Sundararaman, P., & Schoell, M. (1986). Sensitivity of biomarker properties to depositional environment and/or source input in the Lower Toarcian of SW-Germany. *Organic Geochemistry*, 10(4–6), 915–926.
- Niu, J., & Hu, J. (1999). Formation and distribution of heavy oil and tar sands in China. *Marine and Petroleum Geology*, 16(1), 85–95.
- Park, M., Kil, Y., Choi, J., Seol, J., & Kim, J. (2018). Biodegradation characteristics of bitumen from the Upper Devonian carbonates (Grosmont and Nisku formations) in Alberta, Canada. *Geosciences Journal*, 22(5), 751–763.
- Pattan, J. N., & Pearce, N. J. G. (2009). Bottom water oxygenation history in southeastern Arabian Sea during the past 140 ka: Results from redox-sensitive elements. *Palaeogeography, Palaeoclimatology, Palaeoecology*, 280(3–4), 396–405.
- Peters, K. E., & Cassa, M. R. (1994). Applied source rock geochemistry. In: L. B. Magoon & W. G. Dow (Eds.), *The petroleum system—from source to trap* (Vol. 60, pp. 93–120). Tulsa: AAPG.
- Peters, K. E., & Moldowan, J. M. (1993). The biomarker guide: Interpreting molecular fossils in petroleum and ancient sediments. *Choice Reviews Online*, 30(5), 30–2690. <https://doi.org/10.5860/choice.30-2690>.
- Peters, K. E., Walters, C. C., & Moldowan, J. M. (2004). *The biomarker guide*. Cambridge: Cambridge University Press. <https://doi.org/10.1017/cbo9780511524868>.
- Peters, K. E., Walters, C. C., & Moldowan, J. M. (2005). *The biomarker guide. Biomarkers & isotopes in petroleum systems & earth history* (2nd ed., p. 490). <https://doi.org/10.1017/cbo9780511524868>.
- Peters, K. E., Walters, C. C., & Moldowan, J. M. (2017). Biomarkers: assessment of petroleum source–rock age and depositional environment. In *Encyclopedia of petroleum geoscience*.

- Pi, H. J., Hangya, B., Kvitsiani, D., Sanders, J. I., Huang, Z. J., & Kepecs, A. (2013). Cortical interneurons that specialize in disinhibitory control. *Nature*, *503*(7477), 521.
- Qin, J., Wang, S., Sanei, H., Jiang, C., Chen, Z., Ren, S., et al. (2018). Revelation of organic matter sources and sedimentary environment characteristics for shale gas formation by petrographic analysis of middle Jurassic Dameigou formation, northern Qaidam Basin, China. *International Journal of Coal Geology*, *195*(1), 373–385.
- Rabbani, A. R., & Kamali, M. R. (2005). Source rock evaluation and petroleum geochemistry, offshore SW Iran. *Journal of Petroleum Geology*, *28*(4), 413–428.
- Radke, M., Welte, D. H., & Willsch, H. (1986). Maturity parameters based on aromatic hydrocarbons: Influence of the organic matter type. *Organic Geochemistry*, *10*(1–3), 51–63.
- Radke, M., Willsch, H., Leythaeuser, D., & Teichmüller, M. (1982). Aromatic components of coal: Relation of distribution pattern to rank. *Geochimica et Cosmochimica Acta*, *46*(10), 1831–1848.
- Reimann, C., de Caritat, P., Niskavaara, H., Finne, T. E., Kashulina, G., & Pavlov, V. A. (1998). Comparison of elemental contents in O- and C-horizon soils from the surroundings of Nikel, Kola Peninsula, using different grain size fractions and extractions. *Geoderma*, *84*(1–3), 65–87.
- Seifert, W. K., & Moldovan, J. M. (1978). Applications of steranes, terpanes and monoaromatics to the maturation, migration and source of crude oils. *Geochimica et Cosmochimica Acta*, *42*(1), 77–95.
- Shu, D., Xu, S., Wu, S., Li, S., Wang, D., Xiao, Y., et al. (2017). Jurassic sedimentary provenances of the Hongshan and Huobuxun sags in the eastern segment of the northern Qaidam Basin: Basin-Mountain coupling. *Geological Journal*, *52*, 380–393.
- Silva, R. S., Aguiar, H. G., Rangel, M. D., Azevedo, D. A., & Neto, F. R. A. (2011). Comprehensive two-dimensional gas chromatography with time of flight mass spectrometry applied to biomarker analysis of oils from Colombia. *Fuel*, *90*(8), 2694–2699.
- Sinninghe, D., & De, L. (1990). Analysis, structure and geochemical significance of organically-bound sulphur in the geosphere: State of the art and future research. *Organic Geochemistry*, *16*(4–6), 1077–1101.
- Sudiptya, B., & Berna, H. (2018). Flow control devices in SAGD completion design: Enhanced heavy oil/bitumen recovery through improved thermal efficiency. *Journal of Petroleum Science and Engineering*, *169*, 297–308.
- Ten, H., De, L., Rullkötter, J., & Damsté, J. S. (1987). Restricted utility of the pristane/phytane ratio as a palaeoenvironmental indicator. *Nature*, *330*(6149), 641.
- Tenenbaum, D. J. (2009). Oil sands development: A health risk worth taking? *Environmental Health Perspectives*, *117*(4), A150.
- Tian, J., Li, J., Pan, C., Tan, Z., Zeng, X., Guo, Z., et al. (2018). Geochemical characteristics and factors controlling natural gas accumulation in the northern margin of the Qaidam Basin. *Journal of Petroleum Science and Engineering*, *160*, 219–228.
- Wang, J., Feng, L., Steve, M., Tang, X., Gail, T. E., & Mikael, H. (2015). China's unconventional oil: A review of its resources and outlook for long-term production. *Energy*, *82*, 31–42.
- Wang, Y., Zheng, J., Zhang, W., Li, S., Liu, X., Yang, X., et al. (2012). Cenozoic uplift of the Tibetan Plateau: Evidence from the tectonic-sedimentary evolution of the western Qaidam Basin. *Geoscience Frontiers*, *3*(2), 175–187.
- Waseda, A., & Nishita, H. (1998). Geochemical characteristics of terrigenous and marine-sourced oils in Hokkaido, Japan. *Organic Geochemistry*, *28*(1–2), 27–41.
- Wentzel, A., Ellingsen, T. E., Kotlar, H. K., Zotchev, S. B., & Throne-Holst, M. (2007). Bacterial metabolism of long-chain n-alkanes. *Applied Microbiology and Biotechnology*, *76*(6), 1209–1221.
- Wilhelms, A., & Larter, S. (2004). Shaken but not always stirred. Impact of petroleum charge mixing on reservoir geochemistry. *Geological Society, London, Special Publications*, *237*(1), 27–35.
- William, K., Cristiana, L., Nigel, J., Geoff, J., Holly, F., Steve, J., et al. (2018). Petrography and trace element signatures of iron-oxides in deposits from the Middleback Ranges, South Australia: From banded iron formation to ore. *Ore Geology Reviews*, *93*, 337–360.
- Yang, Y., Zhang, B., Zhao, C., & Xu, T. (2004). Mesozoic source rocks and petroleum systems of the northeastern Qaidam basin, northwest China. *AAPG Bulletin*, *88*(1), 115–125.
- Yi, D., Wang, J., Shi, Y., Sun, X., Ma, X., Wang, P., et al. (2017). Evolution characteristic of gypsum-salt rocks of the upper member of Oligocene Lower Ganchaigou Fm in the Shizigou area, western Qaidam Basin. *Natural Gas Industry B*, *4*(5), 390–398.
- Yin, A., Dang, Y. Q., Wang, L. C., Jiang, W. M., Zhou, S. P., Chen, X. H., et al. (2008). Cenozoic tectonic evolution of Qaidam basin and its surrounding regions (Part 1): The southern Qilian Shan-Nan Shan thrust belt and northern Qaidam basin. *Geological Society of America Bulletin*, *120*(7–8), 813–846.
- Zhou, S., Huang, H., & Liu, Y. (2008). Biodegradation and origin of oil sands in the Western Canada Sedimentary Basin. *Petroleum Science*, *5*(2), 87–94.
- Zhou, J., Xu, F., Wang, T., Cao, A., & Yin, C. (2006). Cenozoic deformation history of the Qaidam Basin, NW China: Results from cross-section restoration and implications for Qinghai-Tibet Plateau tectonics. *Earth and Planetary Science Letters*, *243*(1–2), 195–210.